1-1-2011

Characterizing the VAC14 multimeric state

Shannon Cheuk Ying Ho
Ryerson University

CHARACTERIZING THE VAC14 MULTIMERIC STATE

by

Shannon Cheuk Ying Ho

Honours Bachelors of Science

University of Toronto, Ontario, Canada 2009

A thesis presented to Ryerson University

in partial fulfillment of the requirements for the degree of

Master of Science in the Program of

Molecular Science

Toronto, Ontario, Canada, 2011

Author's Declaration

I hereby declare that I am the sole author of this thesis.

I authorize Ryerson University to lend this thesis to other institutions or individuals for the purpose of scholarly research.

_____

I further authorize Ryerson University to reproduce this thesis by photocopying or by other means, in total or in part, at the request of other institutions or individuals for the purpose of scholarly research.

_____

Abstract

Characterizing the Vac14 Multimeric State

Shannon Cheuk Ying Ho, Ryerson University, 2011, Master of Science in Molecular Science

PtdIns(3,5)P_2 is involved in a number of cellular processes, such as the regulation of endolysosome morphology and membrane trafficking, autophagy and ion transport [37]. In mammala, PtdIns(3,5)P_2 deficiency results in vacuolation most notably in the neurons of the central and peripheral nervous system [12, 78]. This can potentially block the trafficking of neurotransmitters leading to a progression of neurodegeneration diseases such as amyotrophic lateral sclerosis and Charcot-Marie-Tooth disease. PtdIns(3,5)P_2 is synthesized by the Fab1/PIKfyve lipid kinase and degraded by the Fig4/Sac3 lipid phosphatase. Fab1 and Fig4 are found in a complex with its regulator, the Vac14/ArPIKfyve adaptor protein. [37]. The aim of this study was to identify the multimeric state of recombinant Vac14 in order to help elucidate the importance of the Vac14 multimer in the regulation of PtdIns(3,5)P_2. The result of this study indicated that recombinant Vac14 forms a homodimer and/or homotrimer.

Acknowledgement

I would like to thank a variety of people who supported me through my master thesis. I would like to thank Dr. Roberto Botelho for giving me the opportunity to work as a part of his lab. Dr. Botelho was crucial to the success of my thesis by providing me guidance and support from his own professional experience throughout my research. I would also like to thank Dr. Debora Foster and Dr. John Marshall for being on my supervisory committee and sharing with me their expertise along the way. Thanks to all my fellow lab mates throughout these two years and my dear friends in the program for their friendliness and companionship that helped make working at the lab enjoyable every day. I would also like to thank Ryerson University for giving me the opportunity to pursue my thesis and for providing me the resources to attain my goals. Last but not least, I would like to thank my family and friends for their support inside and outside of the lab, which helped strengthen and bolster me every day for the tasks ahead, and kept my spirits high when I was at difficult points in my research.

Table of Contents

List of Table

List of Figures

List of Abbreviations Used

ALS	Amyotrophic lateral sclerosis
BME	β-mercaptoethanol
BSA	Bovine serum albumin
CMT	Charcot-Marie-Tooth disease
EEA1	Early endosome antigen 1
ESCRT	Endosomal sorting complexes required for protein transport
FPLC-SEC	Fast protein liquid chromatography with Size exclusion chromatography
GST	Glutathione S-transferase
IP	Immunoprecipitation
LB	Luria-Bertani
MPR	mannose 6-phosphate receptor
MVB	Multivesicular bodies
PCR	Polymerase chain reaction
PH	Pleckstrin homology
PtdIns	Phosphatidylinositol
PtdIns(3)P	Phosphatidylinositol 3-phosphate
PtdIns(3,5)P_2	Phosphatidylinositol-3,5-bisphosphate
PtdIns(4)P	Phosphatidylinositol 4-phosphate
PtdIns(4,5)P_2	Phosphatidylinositol-4,5-bisphosphate
PtdInsP	Phosphoinositides
PX	Phox
SB	Super broth
TBS	Tris buffered saline
TCA	Trichloroacetic acid
TEV	Tobacco Etch Virus
TGN	Trans-Golgi network
TRPML1	mucolipin transient receptor potential proteins

1. Introduction

1.1 The eukaryotic cell

Eukaryotic cells are characterized by a variety of membrane-bound organelles of specialized form and function. This membrane compartmentalization provides different local environments that segregate specific metabolic functions that are often incompatible with each other, like protein synthesis in the endoplasmic reticulum and protein degradation in lysosomes. Membrane-bound organelles are related either through direct physical continuity, like the nuclear envelope and the endoplasmic reticulum, or by the transfer of membrane segments and specific molecules through vesicles in a process called membrane trafficking (Figure 1.1). Membrane trafficking is a multi-step process that involves the transport of membrane and molecules from one organelle to another [74]. This continuous transport of vesicles is important for the precise control of complex cellular processes such as signal transduction, cell division and cell survival. Thus, understanding the process that regulates membrane trafficking and organelle function is important.

1.2 Membrane trafficking

Membrane trafficking begins with the recognition of cargos for transport (Figure 1.1C). Cargos often contain small peptide sequences, such as tyrosine-based motifs, or proteins like ubiquitin, that serve as signals for the recruitment of proteins involved in membrane fission [64]. Proteins that are recruited, such as clathrin and adaptor protein 2 (AP2), assemble into a complex that sorts cargo and bends membranes to form a vesicle (Figure 1.1D) [62]. Membrane fission then occurs to separate the coated vesicles containing cargo from the membrane [78]. Endocytosis is an example of membrane fission, in which a membrane segment of the plasma membrane invaginates toward the interior of the cell and pinches off to form an endocytic vesicle

containing, but not limited, to, nutrient and growth factor receptors [19]. Another example would be the formation of a transport vesicle from the endoplasmic reticulum to transport newly synthesized proteins to other organelles, such as the Golgi for post-translational modifications (Figure 1.1A) [33, 46].

The vesicular transport to target organelles requires membrane targeting. Membrane targeting involves specific proteins, like GTPases, present on the vesicle surface to mediate vesicle interaction with microtubule-associated motor proteins such as, kinesin and dynein, for the active transport to its targeted organelle [2, 20, 36, 39, 50]. To continue with previous examples, the newly derived endocytic vesicle from the plasma membrane is transported to early endosomes (Figure 1.1E), while the transport vesicle from the endoplasmic reticulum is targeted to the Golgi (Figure 1.1A). Multiple tethering proteins and complexes are then required to facilitate the initial contact between transport vesicle and the target membranes, ensuring the proper delivery of vesicles to target membranes [83].

The final event in membrane trafficking is membrane fusion, the process of merging the transport vesicle membrane with the target organelle, thereby depositing molecules within the vesicle into the lumen of the target organelle. Membrane fusion involves a series of complex protein interactions between specific Rab GTPases, tethering proteins and SNARE proteins that facilitate the recognition and docking of the vesicle to the target organelle and finally membrane fusion to form one continuous compartment [48]

Among the many components involved in membrane trafficking, the conserved protein families of the Rab and ARF (ADP-ribosylation factor) GTPases, and the lipid phosphoinositides (PtdInsP), which are derivatives of phosphatidylinositol (PtdIns), contribute significantly in controlling specific steps during cargo selection, vesicle formation, targeting, and fusion.

Consequently, and in addition, the GTPases and the PtdInsPs help establish the distinct properties of organelles, or organelle identity.

1.3 Organelle identity: Phosphoinositides

Organelle identity refers to the unique biochemical, biophysical and functional properties of each organelle, which is endowed by its molecular composition. Two major factors that facilitate organelle identity are the Rab and Arf GTPases and PtdInsPs. Both the GTPases and PtdInsPs recruit specific effector proteins to the cytosolic surface of organelles thereby contributing to organelle identity.

PtdInsPs are central players in membrane trafficking, as well as signal transduction and cytoskeletal rearrangements [18, 51]. PtdInsPs are the phosphorylated derivatives of PtdIns. PtdIns is a phospholipid that consists of a glycerol backbone with two non-polar fatty acid groups attached to position 1 and 2 of the glycerol and an inositol polar head group attached to position 3 of the glycerol backbone (Figure 1.2A). The non-polar fatty acid groups are embedded in the cytosolic leaflet of membrane bilayer anchoring the inositol polar head group in the cytosol. The inositol head group can be phosphorylated on the three, four, and/or five hydroxyl positions to give seven species (Figure 1.2B). The seven species of PtdInsPs are rapidly interconverted through the action of lipid kinases and phosphatases on the cytoplasmic face of specific organelles.

Each PtdInsP is phosphorylated by a specific kinase that recognizes the phosphorylated inositol head group. The kinases can be categorized into 3 types: phosphoinositide 3-kinases (PtdIns3K), phosphoinositide 4-kinases (PtdIns4K), and PtdInsP kinases [41]. Within each category, there are specific kinases for generating individual PtdInsP. For example, Vps34 in yeast, is a PtdIns3K for phosphorylating the 3-OH position of PtdIns to generate

phosphatidylinositol 3-phosphate (PtdIns(3)P), while other PtdIns3Ks are responsible for phosphorylating the 3-OH positions of phosphatidylinositol 4-phosphate (PtdIns(4)P), and phosphatidylinositol-4,5-bisphosphate (PtdIns(4,5)P_2) [4].

There are also specific PtdInsP phosphatases for hydrolyzing the 3-, 4-, or 5-phosphorylated inositol phosphates. Most PtdInsP phosphatases can be categorized into two types: phosphatase that contains only a Sac domain or a Sac domain as well as a PtdInsP 5-phosphatase domain [54]. The Sac domain has activity mainly towards phosphatidylinositol monophosphates; however, the specificity of each Sac domain is dependent on the localization of individual PtdInsP phosphatases. For example, mammalian Sac1 is an integral membrane protein found in the ER that hydrolyzes the 4-phosphate, while yeast Fig4 is a soluble phosphatase that interacts with proteins for its localization to the vacuole to hydrolyze the 5-phosphate of phosphatidylinositol-3,5-bisphosphate (PtdIns(3,5)P_2) [54, 56].

Each PtdInsP exhibits a particular organellar distribution and participates in the recruitment of specific set of cognate proteins. Thus, PtdInsPs help distinguish each organelle at the molecular and functional level. To increase avidity of effectors to associate with organelle surfaces, effectors can bind to both GTPases and PtdInsPs at the same time, contributing to coincidence detection. For example, the four-phosphate-adaptor protein involved in cargo transfer from trans-Golgi network (TGN) to the plasma membrane, require association with both PtdIns(4)P and Arf1 on the TGN [32]. Therefore, the different combination of PtdInsP and GTPases required for the recruitment of specific protein effectors provide each organelle with a unique organelle identity.

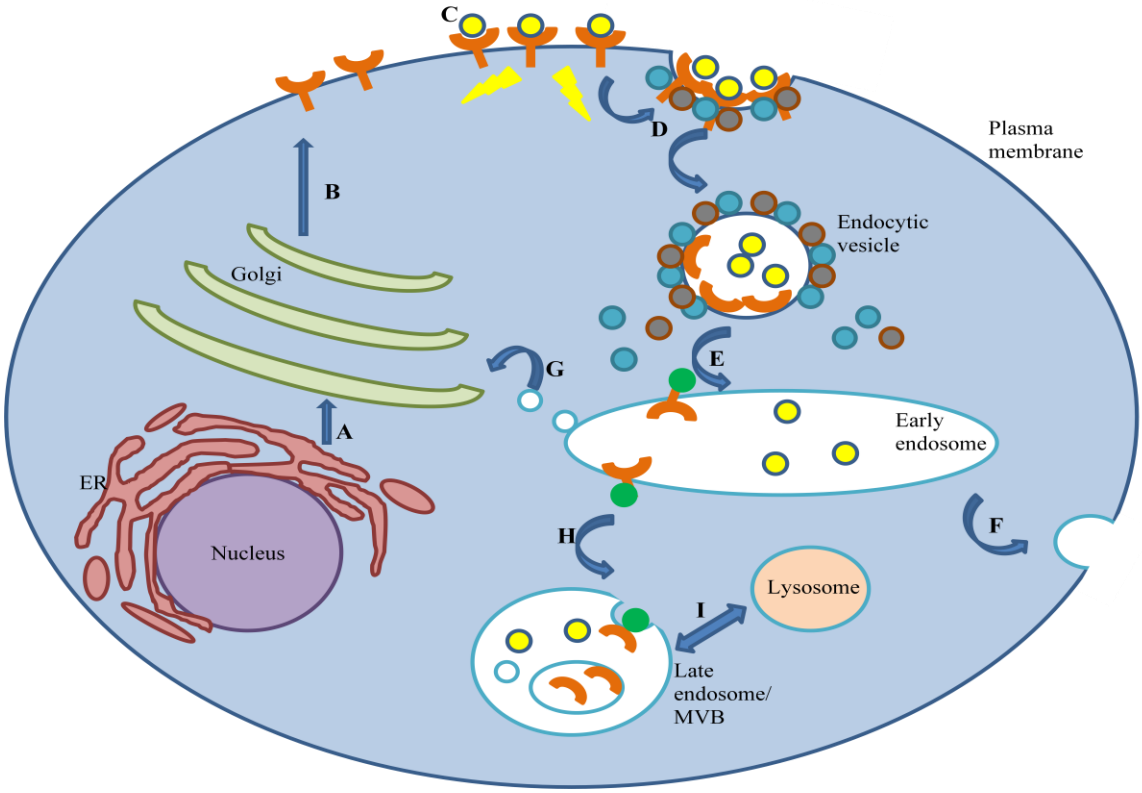

Figure 1.1 Summary of membrane trafficking in a typical eukaryotic cell. The endoplasmic reticulum (ER) is interconnected with the nucleus and synthesizes proteins for delivery to the Golgi in transport vesicles (A). The Golgi post-modifies proteins for transport to the plasma membrane and other organelles (B). Ligand binding to surface receptor initiates both signal cascades involve in multiple cellular events (C) and binding of proteins, such as clathrin, adaptor protein 2, to intracellular tail of the receptor, to initiate endocytosis and fission to generate an endocytic vesicle (D). Endocytic vesicle is transported to and fuses with the early endosome (E). Molecules in the early endosome can be recycled back to the plasma membrane (F) or the Golgi (G). Molecules in the early endosome destined for degradation are mono-ubiquitinated and internalized into multivesicular bodies (MVB), which then matures into a late endosome (H). Lysosome containing proteases fuses with the late endosome/MVB for the degradation of molecules (I).

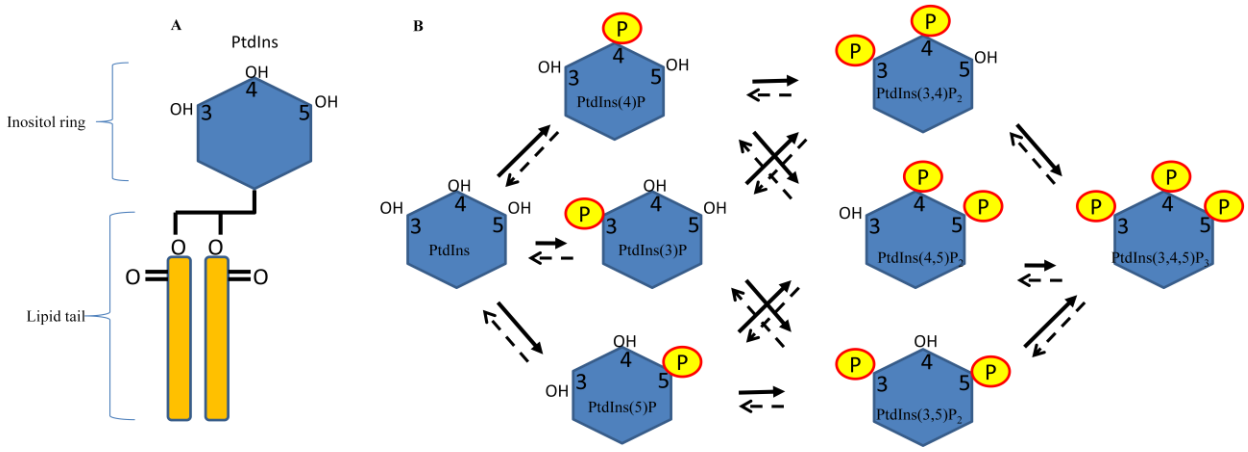

Figure 1.2. Phosphoinositides, the derivatives of phosphatidylinositol. Phosphatidylinositol (PtdIns) consisted of an inositol head group connected to a lipid tail through a glycerol backbone (A). The inositol ring can be phosphorylated at the 3-, 4-, and/or 5-OH group to generate 7 different phosphoinositides (PtdInsP) and can be interconverted by the actions of specific lipid kinases (solid arrows) and lipid phosphatases (broken arrows) (B)

1.4 The endocytic pathway: The role of phosphoinositides

Upon membrane receptor stimulation by extracellular ligands, such as the binding of transferrin to transferrin receptors on the plasma membrane, ARF6 recruits PtdIns(4)P-5 kinase for the phosphorylation of PtdIns(4)P to PtdIns(4,5)P_2 [49]. PtdIns(4,5)P_2 promotes endocytosis by interacting with pleckstrin homology (PH) domains of effector proteins, such as clathrin and dynamin (a large GTPase) that functions to promote vesicle deformation and fission, respectively (Figure 1.1D) [79]. Rab5 is also recruited to the budding vesicle for the effective sequestration of transferrin into the vesicle in addition to recruiting subsequent effector proteins (see below) [40, 58].

After formation of the endocytic vesicle, PtdIns(4,5)P_2 is converted to PtdIns by synaptojanin 1, a lipid phosphoinositide phosphatase with 5- and 4-phosphatase domains [17, 59]. Rab5 on the endocytic vesicle recruits class III phosphoinositide 3-kinase (or Vps34p, the yeast homolog) for the generation of PtdIns(3)P on the endocytic vesicle. Effector proteins are

recruited to endocytic vesicle by interacting with PtdIns(3)P through their FYVE domain (a conserved zinc-finger) or Phox (PX) domain (a conserved polyproline motif (PxxP)) [28, 75]. In some cases, effector proteins such as the early endosome antigen 1 (EEA1) require interaction with both PtdIns(3)P and Rab5 for localization to the endocytic vesicles and early endosomes, an example of coincidence detection. EEA1 and SNAREs are among the proteins that facilitate endocytic membrane tethering and fusion, respectively [14, 75].

Another Rab GTPase, Rab4, is also located on early endosomes and regulates recycling of cargo molecules, such as transferrin receptors back to the plasma membrane (Figure 1.1 F) [57]. During recycling of cargo molecules, multiple fission events from early endosomes concentrate molecules for degradation. Cargo molecules targeted for degradation have mono-ubiquitin conjugated to their cytosolic domains. The ESCRT (**E**ndosomal **S**orting **C**omplexes **R**equired for protein **T**ransport) machinery consisted of four ESCRT protein complexes (ESCRT-0, ESCRT-I, ESCRT-II, and ESCRT-III) are recruited to the early endosomes by interacting with the ubiquitylated cargos, the ESCRT-0 also contain a FYVE domain that interacts specifically with PtdIns(3)P on early endosome [65]. The ESCRTs are responsible for sorting and internalization of ubiquitylated endosomal proteins into internal vesicles in the endosomes for eventual degradation [66]. Endosomes containing multiple internal vesicles are known as multivesicular bodies (MVB) (Figure 1.1H). The MVB is an intracellular organelle that stores proteins destined for degradation, which eventually fuses with the late endosome and lysosome (Figure 1.1I), where the proteins are degraded by hydrolytic enzymes, such as proteases [8].

1.5 Phosphatidylinositol-3,5-bisphosphate (PtdIns(3,5)P_2)

During the transport of endosomal cargo to the late endosome, PIKfyve, a PtdIns(3)P 5-kinase (or Fab1, the yeast homolog), is recruited to PtdIns(3)P through its FYVE domain, to generate PtdIns(3,5)P_2 [16, 31]. PtdIns(3,5)P_2 is the predominant phosphoinositide found on the late endosomal membrane of mammalian cells, and on the vacuolar membrane of yeast [61]. PtdIns(3,5)P_2 constitutes about 0.08% of the total PtdInsP in yeast and less than ~0.05% in mammalian cells but it is postulated to be involved in a variety of cellular functions for the survival of the cell [22, 25, 86].

In yeast, PtdIns(3,5)P_2 is currently known to regulate morphology and acidification of the vacuole, formation of specific MVB populations and, recycling of the cargo molecules from the vacuole [23, 31, 84]. In yeast, during hyperosmotic shock, there is a 20-fold increase in the level of PtdIns(3,5)P_2 generated by the PtdIns(3)P 5-kinase, Fab1 (see below), to regulate cell homeostasis [16, 22, 25, 31]. In the absence of PtdIns(3,5)P_2, the vacuole of yeast is enlarged (Figure 1.3B). The enlarged vacuole may be a consequence of membrane accumulation due to reduced recycling of cargo molecules and/or inability to form MVB [9].

The functions of PtdIns(3,5)P_2 is conserved in higher eukaryotes. Mammalian cells deficient in PtdIns(3,5)P_2 also have enlarged late endolysosomal structures (Figure 1.3D) [23, 43, 44, 63]. The enlarged late endocytic structures in mammalian cells may be a consequence of reduced retrograde membrane trafficking from late endosome in the absence of PtdIns(3,5)P_2 [70]. For example, mannose 6-phosphate receptor (MPR) and sortilin are known receptors that undergo retrograde trafficking from the endosomes to TGN. In the absence of PtdIns(3,5)P_2, there is a 77.2±13.3% and 54.6±19.6% reduction in retrograde transport of MPR and sortilin to the TGN, respectively [11, 70]. PtdIns(3,5)P_2 has been found to interact and activate the Ca^{2+}

channel, mucolipin transient receptor potential proteins (TRPML1), through a poly-basic region [21]. Over-expression of the calcium channel, TRPML1, rescued the enlarged endolysosome structure in PtdIns(3,5)P_2-deficient mouse fibroblasts, implicating involvement of Ca^{2+}-mediated membrane fusion and fission events [21]. A defect in membrane fusion and fission can affect retrograde trafficking possibly retarding the down-regulation and/or recycling of protein receptors for a variety of cellular functions [26, 29, 31, 69]. Importantly, defect in retrograde trafficking and the presence of enlarged endolysosomal structures due to mutations in PtdIns(3,5)P_2 regulators, resulted in vacuolation and degeneration in both motor and sensory neurons in mice (Figure 1.3A and D). Vacuolation seems to block traffic along the neuron axons. This is speculated to be linked to several human neuropathologies, such as Charcot-Marie-Tooth Disease (CMT) and amyotrophic lateral sclerosis (ALS) [12, 13, 85, 86]. To better understand the actions of PtdIns(3,5)P_2, it is important to decider the molecular mechanisms involve in its regulation.

1.6 Regulation of PtdIns(3,5)P_2

To understand PtdInsPs action, it is essential to define the mechanisms underlying the synthesis of PtdInsPs by lipid kinases and phosphatases. PtdIns is first phosphorylated at the 3-hydroxyl position by Vps34p, a PtdIns 3-kinase, into PtdIns(3)P, which is responsible for protein sorting and maturation of the endosomes (as indicated above) [87]. PtdIns(3)P is then phosphorylated at the 5-hydroxyl position by a PtdIns(3)P 5-kinase, Fab1/PIKfyve, into PtdIns(3,5)P_2 (Figure 1.4) [31]. A lipid phosphatase, Sac3 in mammalian cells, or Fig4 in yeast, converts PtdIns(3,5)P_2 back to PtdIns(3)P (Figure 1.4). PtdIns(3,5)P_2 can also be dephosphorylated to PtdIns(5)P by myotubularin, a phosphoinositide 3-phosphatase [67]. PtdInsP kinases and phosphatases are themselves regulated by many types of proteins. Vac14 in

yeast (or ArPIKfyve in mammalian cells) is the positive regulator of Fab1 (Figure 1.4) [30, 73]. In addition to regulating Fab1, Vac14 also acts as a recruiter of Fig4 on the vacuole of yeast (or late endocytic structures in mammalian cells) (Figure 1.4) [68, 73].

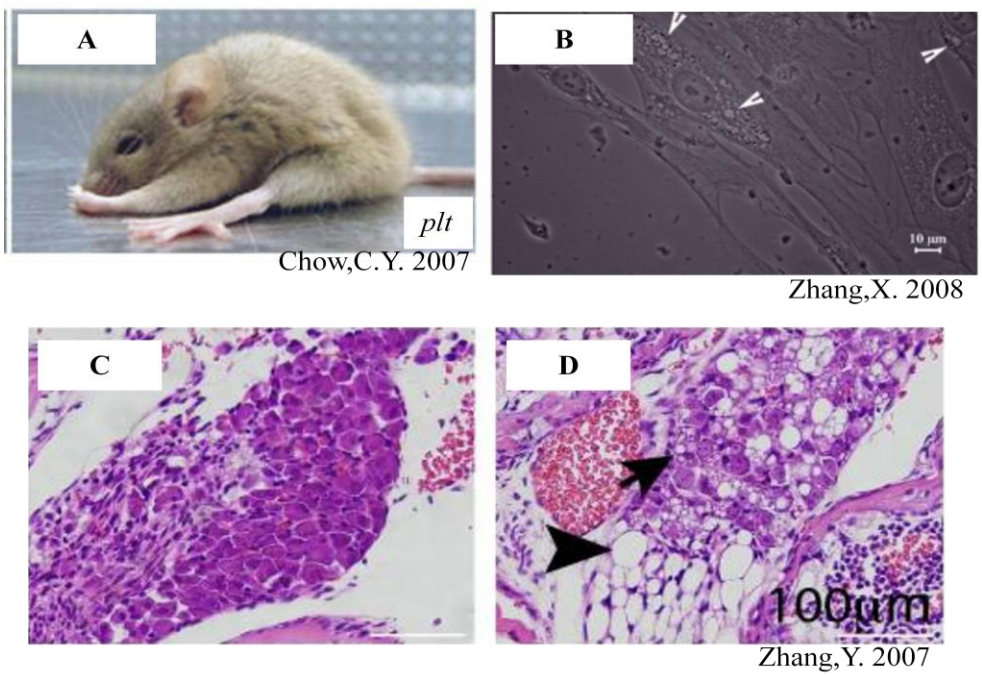

Figure 1.3. Mammalian cells deficient in PtdIns(3,5)P_2. *Pale tremor* (*plt*) mice deficient in PtdIns(3,5)P_2 due to presence of a mutation in Fig4 similar to mutation found in CMT4J-related patients (A) [13]. Fibroblast culture from CMTAJ-patients containing vacuolations (white arrow head) (B) [85]. Dorsal root ganglion of wild-type mice (C) [86]. Dorsal root ganglion of *βgeo/βgeo* mice deficient in PtdIns(3,5)P_2 due to absence of Vac14 (D) [86]. Intracellular vacuolation (black arrow) and single vacuole filling the whole cell body (black arrow head).

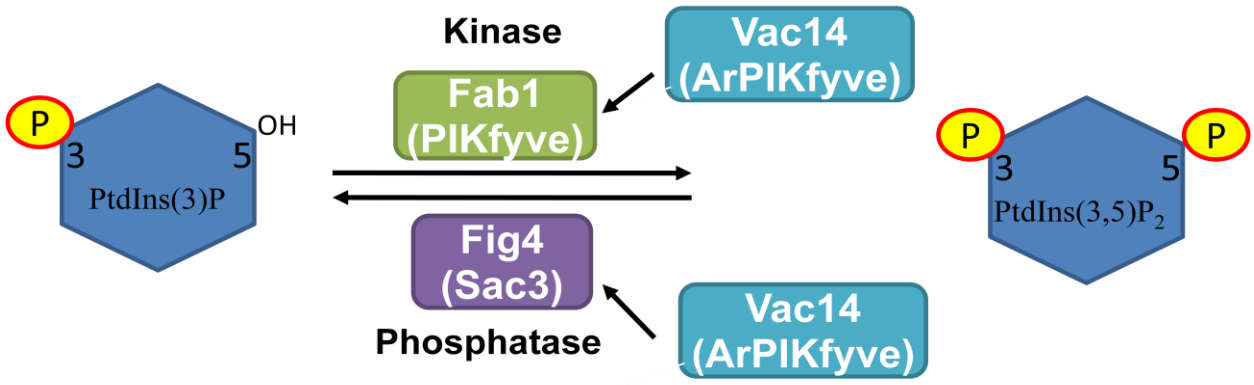

Figure 1.4. Regulation of PtdIns(3,5)P_2. PtdIns(3)P is phosphorylated at the 5-hydroxyl position by the yeast Fab1 kinase, or the mammalian ortholog PIKfyve, to generate PtdIns(3,5)P_2. PtdIns(3,5)P_2 can be dephosphorylated back to PtdIns(3)P by the yeast Fig4 phosphatase, or the mammalian ortholog, Sac3. The yeast Vac14, or the mammalian ortholog ArPIKfyve, is the adaptor protein that is required for the function of both the Fab1/PIKfyve and Fig4/Sac3.

1.6.1 Fab1: Phosphatidylinositol 3-phosphate 5-kinase

Fab1/PIKfyve, is a 257kDa protein that contains highly conserved domains: the N-terminal FYVE domain, the CCT and CCR domains, and the C-terminal lipid kinase domain (Figure 1.5A) [6, 31, 38]. The lipid kinase domain of Fab1 is most closely related to PtdIns(4)P 5-kinase and PtdIns(5)P 4-kinase [16, 31, 84]. Fab1 kinase dead mutant showed comparable results to *fab1Δ;* an undetectable levels of PtdIns(3,5)P_2 and enlarged vacuoles (Figure 1.5B), demonstrating that the Fab1 kinase is solely responsible for the synthesis of PtdIns(3,5)P_2 [6, 16].

FM4-64 is an amphiphilic fluorescent styryl pyridinium dye that binds to the plasma membrane and internalized by constitutive endocytosis [81]. FM4-64 is then transported to the vacuole/lysosomes via the endocytic pathway where it stains the limiting membrane of the vacuole [81]. Fab1 was found to co-localize with FM4-64 on the vacuolar membrane, and mutations on the FYVE domain of the Fab1 kinase resulted in membrane dissociation of Fab1

(Figure 1.5C) [6]. These results suggest that the FYVE domain is responsible for localizing Fab1 to the vacuolar membrane and not the early endosome, as it occurs for other FYVE domain containing proteins like EEA1.

The CCT and CCR domains of Fab1 are related to the GroL superfamily. The GroL superfamily is a family of chaperones that bind and facilitate proper folding of actin and tubulin [82]. Studies using point mutations in the CCR and CCT domains resulted in a 22% and 42% of wild-type level PtdIns(3,5)P_2, respectively, and a moderately enlarged vacuole (Figure 1.5B) [6]. In addition, deletion of the CCT domain resulted in loss of interaction with Fab1 regulators [6]. Thus, the CCT and CCR domains interact with Fab1 regulators, Vac14 and Fig4, to regulate the synthesis of PtdIns(3,5)P_2 (see below) [6].

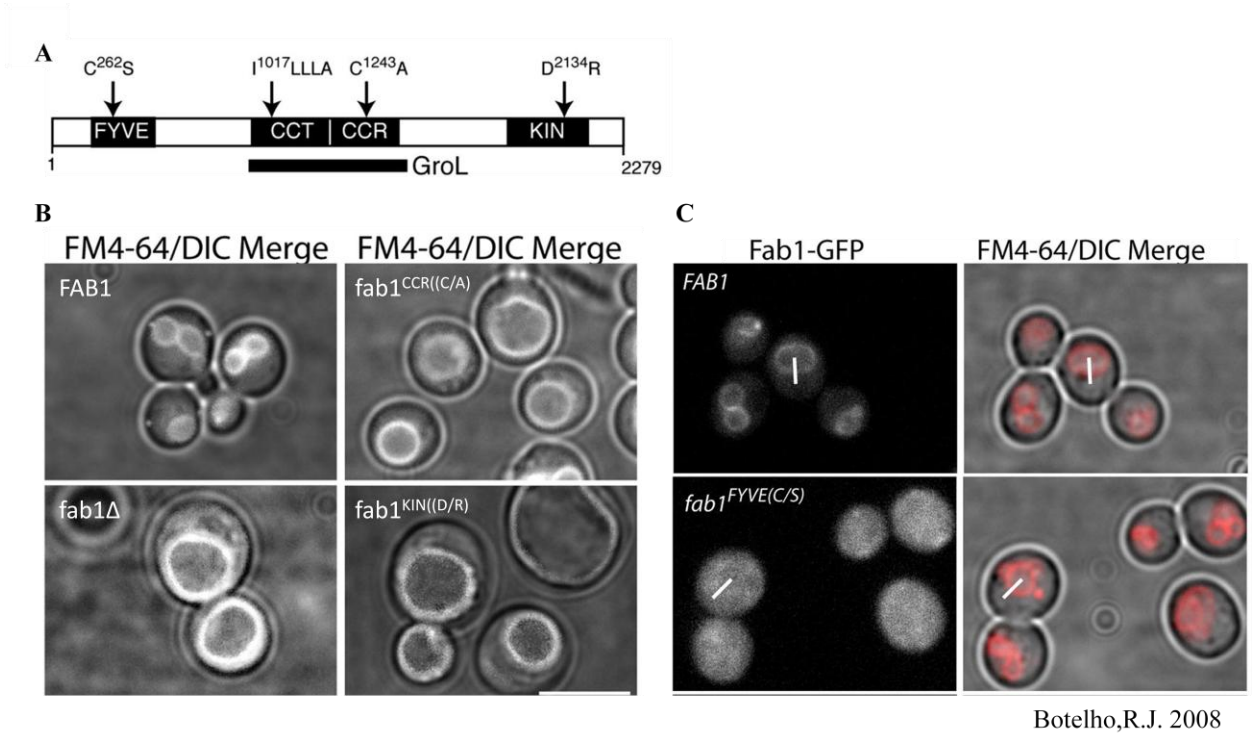

Figure 1.5. Vacuole morphology of Fab1 point mutants and localization of Fab1. Diagram showing the domains of Fab1 (FYVE, GroL (CCT/CCR), and the kinase (KIN)), and the various point mutations (A) [6]. FM4-64/DIC merge images of vacuole morphology of *fab1Δ* yeast cells expression FAB1, fab1$^{CCR(C/A)}$, and fab1$^{KIN(D/R)}$ (B) [6]. Wild-type yeast expression endogenous FAB1-GFP and fab1$^{FYVE(C/S)}$-GFP (C) [6].

1.6.2 Fig4: Phosphatidylinositol-3,5-bisphosphate 5-phosphatase

Fig4 contains a conserved Sac domain, which is a known lipid phosphatase domain. Point mutations in the catalytic domain of Fig4 resulted in 3-fold increase in the levels of PtdIns(3,5)P_2 while the levels of other PtdInsP remained relatively the same, indicating that Fig4 is responsible for dephosphorylating PtdIns(3,5)P_2 [30]. Deletion of Atg18, a negative regulator of PtdIns(3,5)P_2 levels, resulted in a dramatic increase in the level of PtdIns(3,5)P_2 (~0.9% vs. ~0.1% of total PtdInsP in wild-type) [27]. Expression of catalytically inactive Fig4 in the double deletion mutant resulted in even higher levels of PtdIns(3,5)P_2 (~1.37% of total PtdInsP) [6]. However, counter-intuitively, double deletion of Atg18 and Fig4 recreated wild-type level of PtdIns(3,5)P_2 [6]. The paradoxical result of the *fig4Δ* cells is best explained by a model in which Fig4 plays a dual function in the synthesis and degradation of PtdIns(3,5)P_2 [25, 27]. Localization of Fig4 to the vacuolar membrane is dependent on association with Vac14, and vice versa, as well as interaction with Fab1 (see below) [6, 25]. As a result, deletion of Fig4 prevents Vac14 from activating Fab1, thereby reducing the levels of PtdIns(3,5)P_2. Consistent with this paradigm, patients with autosomal recessive Charcot-Marie-Tooth disorder (CMT4J) were found to have mutations in *FIG4* that results in a decrease in PtdIns(3,5)P_2 level [13, 85]. Vacuolation in the late endocytic structures were observed in cultured fibroblasts isolated from a patient with CMT4J (Figure 1.3B). It is suggested that the vacuolation in neurons prevents the trafficking of intracellular organelles resulting in neurodegeneration in motor and sensory neurons of CMT4J patients [85].

1.6.3 The Vac14 adapter protein

Vac14, a ~100kDa protein in yeast, was discovered in a mutant screen for an enlarged vacuolar morphology and a dramatic decrease in PtdIns(3,5)P_2 levels, similar to those observed in Fab1 mutants [5, 23, 25]. The function of Vac14 is conserved in its mammalian counterpart, ArPIKfyve. Mice models deleted for ArPIKfyve showed a drop in PtdIns(3,5)P_2 level and, vacuolation in both the central and peripheral nervous systems which led to neuronal degeneration (Figure 1.3D) [86]. Thus, Vac14 is a regulator of Fab1.

Sequence analysis and multiple sequence alignments with REP, a repeat finding program based on homology using statistical significance estimates, and Pfam database, indicated that Vac14 is mostly composed of HEAT-like repeat domains (Figure 1.6A) [23, 45]. The HEAT repeat motif was named after the first four proteins identified to contain HEAT repeats: **H**untingtin, **E**longation factor 3, regulatory subunit **A** of Protein phosphatase 2A, and protein kinase **T**OR (target of rapamycin) [1]. HEAT repeat is a conserved motif that typically consists of two α-helices connected with a loop (Figure 1.6B). Each repeat can interact with neighbouring HEAT repeats through hydrophobic interactions forming a superhelix that serves as a structural scaffold for protein-protein interactions (Figure 1.6C and D) [1, 47]. Jin et al. postulated that there are at least 9 and up to 21 potential HEAT-like repeat domains in yeast Vac14, and a minimum of 3 and up to 17 potential HEAT-like repeats in ArPIKfyve [23, 45]. Therefore, the HEAT-like repeats present in Vac14 are potential interaction sites with PtdIns(3,5)P_2 regulators like Fab1, Fig4, and possibly with another Vac14 molecule (see below).

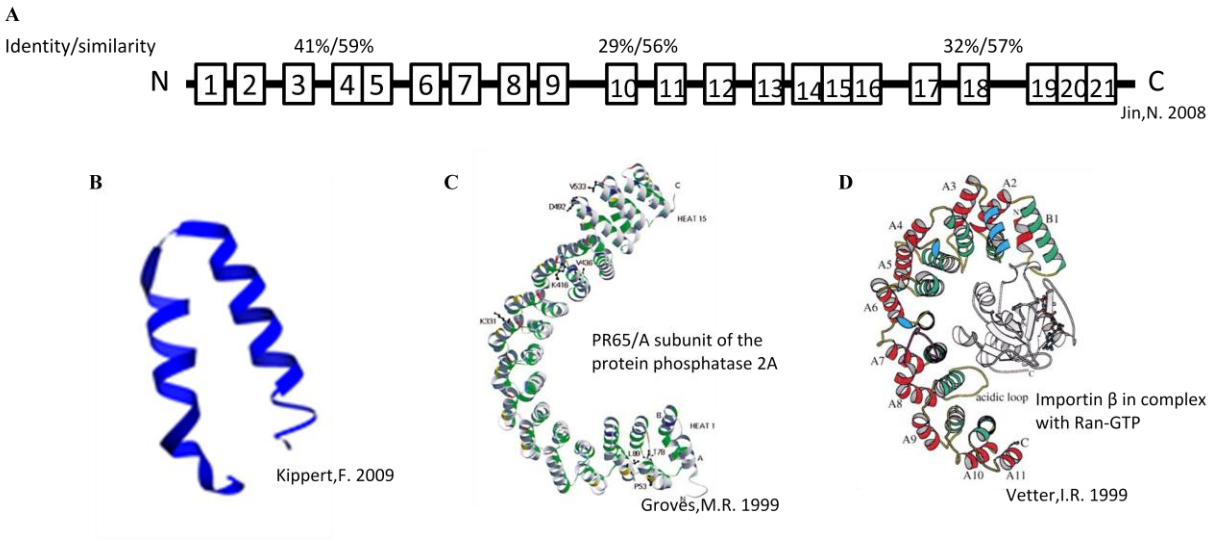

Figure 1.6. Sequence identity and similarity between mammalian and yeast Vac14, and the structure of proteins containing HEAT-repeat motifs. Diagram showing the predicted location of the 21 HEAT repeats in yeast Vac14 by pfam, and the percentage of identity and similarity between mammalian and yeast Vac14 N-terminal, middle, and C-terminal regions are indicated (A) [45]. Ribbons diagram of a single HEAT-repeat motif consisted of two anti-parallel helix connected with a loop (B) [47]. Ribbons diagram of the PR65/A subunit of the protein phosphatase 2A containing 15 HEAT-repeat motifs (C) [35]. Ribbons diagram of the importin β containing 17 HEAT-repeat motifs in complex with the substrate Ran-GTP (D) [80].

Vac14 and Fab1 colocalize in yeast, indicating Vac14 activates Fab1 on the vacuolar membrane [25, 73]. However, to interact with Fab1 on the vacuole, Vac14 is first required to bind the Fig4 phosphatase, in both yeast and mammalian systems. Interestingly, Fig4 also requires Vac14 interaction to localize to vacuole. To observe individual functions of Vac14 and Fig4, *FIG4* and *VAC14* were simultaneously over-expressed in a yeast strain containing *fig4Δ*, *vac14Δ* and having *FAB1* substituted with *fab1-14*, an active mutant containing mutations in the kinase domain [25]. During hyperosmotic shock, the level of PtdIns(3,5)P_2 in *fig4Δvac14Δfab1-14* is similar to wild-type level [25]. Over-expression of either Vac14 or FIG4 alone resulted in no turnover of PtdIns(3,5)P_2. However, when Vac14 and FIG4 are over-expressed together, there is turnover of PtdIns(3,5)P_2 [25]. Thus, association of Vac14 with Fig4 is required for the

recruitment of Fig4 to the vacuolar membrane for dephosphorylation of PtdIns(3,5)P_2. Due to this Vac14-Fig4 interaction, Vac14 and Fig4 play dual roles in PtdIns(3,5)P_2 synthesis and degradation [25, 68].

1.7 The Fab1 complex

One question that remained until recently was how Fab1, Fig4 and Vac14 were coordinated. A possible model of how these proteins "communicated with each other" was obtained through co-immunoprecipitation (co-IP) analysis that demonstrated that Vac14, Fig4 and Fab1 co-immunoprecipitated with each other in several permutations (Figure 1.7) [6, 45]. A series of co-IP analyses were conducted to identify interactions between individual proteins in yeast and mammalian system [6, 42, 72]. Co-IP analysis using *fab1Δ* cells showed that Vac14 and Fig4 still interacted with each other (Figure 1.7B). However, both Fig4 and Vac14 failed to co-IP with Fab1 in *vac14Δ* and *fig4Δ* cells, respectively, suggesting Vac14 and Fig4 are co-dependent for interaction with Fab1 (Figure 1.7C and D) [6, 45].

These observations help to explain how Vac14 and Fig4 have dual functions in synthesis and degradation of PtdIns(3,5)P_2. Vac14 is known to activate Fab1 (binds directly to the GroL-domain) but it is also needed to recruit Fig4 to the vacuolar membrane via the Fab1 complex. In contrast, Fig4 not only acts as a lipid phosphatase but it is needed to secure Vac14 with Fab1. Together, these results suggest that Fab1, Vac14, and Fig4 might exist as a complex regulating the synthesis and turnover of PtdIns(3,5)P_2 on vacuolar membrane. The same interaction also exists in mammalian system for PIKfyve, ArPIKfyve, and Sac3 [42].

Recent studies employing yeast two-hybrid assay and co-IP analyses with mammalian system using Vac14 truncations were able to identify putative regions, possible HEAT repeats on Vac14 that are involved in interaction with Fab1 and Fig4 [42, 45]. Truncated Vac14 containing

the N-terminal half was sufficient for interaction with Fab1, while the C-terminal half was sufficient for interaction with Fig4 [42, 45].

Vac14 appears to serve as a regulatory scaffold in the Fab1 complex helping to regulate the levels of PtdIns(3,5)P_2. To understand how the Fab1 complex regulates the levels of PtdIns(3,5)P_2, it would be appropriate to understand the molecular properties of Vac14.

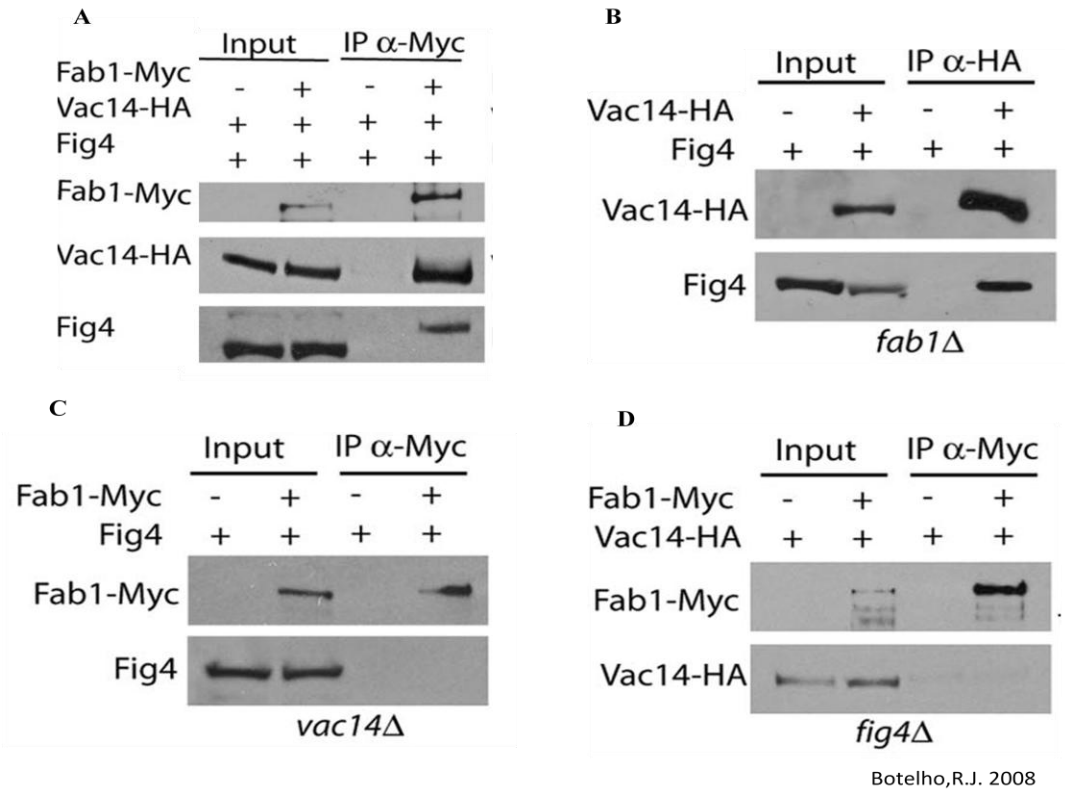

Figure 1.7. Co-IPs of Fab1, Fig4, and Vac14 in yeast. IP with monoclonal α-myc antibody of whole cell lysate from wild-type yeast, *vac14Δ* and *fig4Δ* cells (A, C, and D, respectively) [6]. IP with monoclonal α-HA antibody of whole cell lsyate from *fab1Δ* cells (B) [6].

1.8 The Vac14 multimer

There is evidence indicating that Vac14 interacts with at least another molecule of Vac14 [6, 42, 72]. IP analysis using antibodies against the HA-epitope with whole cell lysates from yeast cells expressing two alleles of Vac14 (HA-Vac14 and Vac14-FLAG) was able to isolate Vac14-FLAG, indicating potential Vac14 self-interaction (Figure 1.8B) [6]. In-vitro analysis also demonstrated that recombinant GST-Vac14 coupled to glutathione-agarose beads interacted with recombinant T7-Vac14-HIS, showing direct interaction (Figure 1.8C) [6].

Similar co-IP studies employing mammalian cells expressing two alleles of ArPIKfyve, also demonstrated a potential ArPIKfyve self-interaction [71]. In-vivo cross-linking of Myc-ArPIKfyve identified three separate protein bands of approximately 82kDa, 170kDa, and 250kDa in size (Figure 1.8A). A monomer of ArPIKfyve is ~82kDa, therefore, it suggest that ArPIKfyve exist as a homomeric protein, possibly a homodimer or a homotrimer [71]. Co-IP with ArPIKfyve truncations also suggested possible ArPIKfyve self-interaction sites to be located at the C-terminal half using truncated ArPIKfyve mutants [71]. However, the analyses done by Sbrissa et al. were not conclusive. First, the truncations employed were relatively large, spanning almost half of the protein. A more defined location of the Vac14 self-interaction site would be more useful for future functional assays. Second, multimeric studies were done in mammalian cells in the presence of other potential ArPIKfyve binding partners, including PIKfyve and Sac3 lipid phosphatase. Sac3 is approximately 90 kDa, thus, it could account for the observed protein bands at ~170 or 250 kDa in the study by Sbrissa, et al (Figure 1.8A).

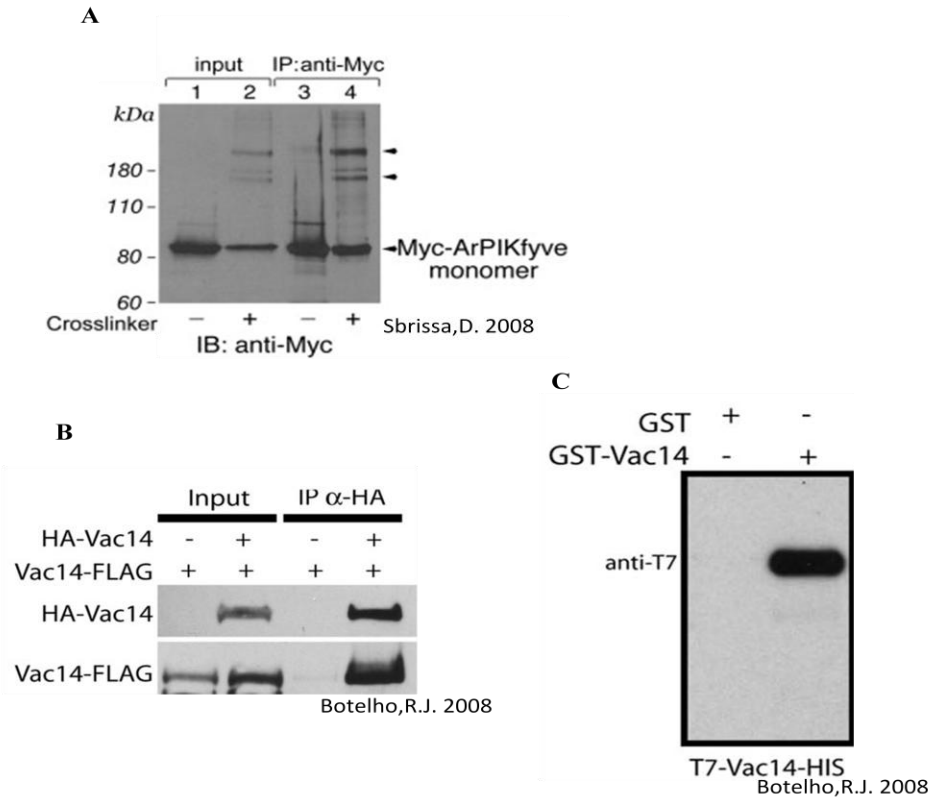

Figure 1.8. Vac14 self-interaction. Myc-ArPIKfyve were cross-linked with methanol-free formaldehyde *in-vivo* and IP with monoclonal α-Myc antibody (A) [71]. Putative myc-ArPIKfyve homodimer and homotrimer at ~170 kDa and ~250 kDa, respectively (arrowhead in A). IP with monoclonal α-HA antibody in yeast expressing both HA-Vac14 and Vac14-FLAG (B) [6]. In-vitro binding assay of purified recombinant GST-Vac14 with recombinant T7-Vac14-HIS (C) [6].

1.9 Hypothesis

Although the results from the mammalian system are not conclusive, they are still in agreement with results from the yeast system and recombinant in-vitro studies, which indicated that Vac14 self-interacts to form a Vac14 multimer. This leads to the hypothesis that Vac14 self-interacts and forms a homomeric complex. I aim to define the multimeric state of Vac14 using the following objectives.

1.10 Objectives

a) Optimize expression and purification of recombinant T7-Vac14-HIS in *E.coli* BL21 DE3 strain.
b) Identify the molecular weight of recombinant T7-Vac14-HIS multimer by fast protein liquid chromatography with size-exclusion chromatography.
c) Identify the molecular weight of recombinant T7-Vac14-HIS multimer by differential velocity ultracentrifugation with glycerol gradient.

1.11 Fast protein liquid chromatography using size-exclusion column

Size exclusion gel chromatography is often used to separate and purify macromolecules from a mixture based on their native molecular weight. Mixture of macromolecules is subjected to a column filled with a porous matrix. The pores within the matrix are designed to allow macromolecules within a certain range of molecular weight to migrate through, known as a fractionation range. The smaller the macromolecule, the probability of it entering the pores increases [77]. Entering the pores will slow down the migration of the macromolecule through the column, delaying the elution of the macromolecule out of the column. As a result, macromolecules will elute in order of decreasing size. However, macromolecules with molecular weights outside of the fractionation range will not be separated efficiently. Macromolecules with molecular weight higher than the fractionation range will not enter the pores, and therefore elute first at equal rate in the void volume. Similarly, macromolecules with molecular weight smaller than the lower end of the fractionation range will enter and stay in the pores with the same probability and they will elute together without separation at the end [77]. The rate of migration through the column is also affected by the Stoke's radius, or the hydrodynamic radius, which refers to the shape of the molecule [55]. Macromolecules that are not globular migrate through a

solution as a hypothetical sphere, as a result, macromolecules that are elongated will acquire a larger radius compared to a globular protein that has a similar molecular weight. The Stoke's radius affects the probability of the macromolecule to enter the porous matrix: as the Stoke's radius increases, the probability of the macromolecule to enter the porous matrix decreases. Thus, the probability of an elongated macromolecule to enter the porous matrix is less than the probability of a globular protein that has a similar molecular weight but a smaller Stoke's radius. [24].

Proteins of known molecular weights, such as catalase (approx. 200kDa), ferritin (approx. 450kDa), and thyroglobulin (approx. 660kDa) will be used to estimate molecular weights of corresponding fractions. The apparent molecular weight of recombinant Vac14 fractions will then be assigned by comparing the fraction numbers to the molecular weight standards. FPLC fractionation should inform us if recombinant T7-Vac14-HIS exists in single multimeric state (dimer or trimer, for example) or if recombinant T7-Vac14-HIS exists in multiple multimeric states (for example, as a monomer and dimer). If the results from FPLC size-exclusion chromatography contain a single peak, this would suggest that there is only one homomeric state of the T7-Vac14-HIS. Results with multiple peaks will indicate recombinant T7-Vac14-HIS exists in multiple multimeric states.

1.12 Differential velocity ultracentrifugation with a glycerol gradient

Differential velocity ultracentrifugation using a glycerol gradient can also be used to estimate the size of the recombinant Vac14 multimer. Different percentages of glycerol are layered on top of one another creating a density gradient, with the more viscous (or higher percentage) glycerol at the bottom. When a cell lysate layered on top of the glycerol gradient is subjected to high centrifugal force, the proteins will differentially migrate through the glycerol

gradient [7]. The migration rates of proteins through the glycerol gradient depend mostly on the molecular weight of the protein. Proteins with higher molecular weight will migrate toward the bottom (higher glycerol concentration) of the glycerol gradient faster than proteins with lower molecular weight due to a higher gravitational force pulling on the larger protein [53]. Proteins with known molecular weight (phosphorylase b, catalase, ferritin, and thyroglobulin) will be used to identify the molecular weight of each fraction. Protein standards and recombinant T7-Vac14-HIS will be simultaneously subjected to velocity ultracentrifugation. The molecular weight of the recombinant T7-Vac14-HIS multimer can be deduced by identifying the protein standard that is found in the same glycerol fraction that also contains recombinant T7-Vac14-HIS.

2. Materials and Methods

2.1 Bacterial strains

DH5α competent cells [F^- φ80*lac*ZΔM15 Δ(*lac*ZYA-*arg*F)U169 *rec*A1 *end*A1 *hsd*R17(r_k^-, m_k^+) *pho*A *sup*E44 *thi*-1 *gyr*A96 *rel*A1 λ^-] (Invitrogen) were used for cloning plasmid DNA. *Escherichia coli* BL21 (DE3) strain [*E. coli* B F^- *dcm ompT hsdS*($r_B^-m_B^-$) gal λ(DE3)] (Stratagene) was used for recombinant protein expression.

2.2 Transformation for cloning and expression

One microliter of 100-300 ng/µl plasmid DNA was added to 50 µl competent BL21 DE3 or DH5α and incubated on ice for 30 mins. Cells were heat shocked at 42°C for 45 sec and incubated immediately on ice for 2 min. One millilitre of Luria-Bertani (LB) media was added to the transformation reaction and incubated at 37°C for 40 min. Two hundred microliters of transformed cells were plated on LB plates containing 100 µg/ml ampicillin and incubated at 37°C overnight.

2.3 Purification of plasmid DNA

Single bacterial colonies were inoculated in 10 ml of LB media supplemented with 100 µg/ml ampicillin and incubated overnight at 37°C with constant agitation. The overnight culture was then centrifuged at 12,000 rpm for 2 min, and the plasmid DNA was extracted using a Plasmid Mini Prep Kit (Bio-Basic Ltd.) as per manufacturers' instructions.

2.4 Plasmids and cloning

T7-Vac14-HIS and GST-Vac14 were previously characterized [6]. Briefly, *VAC14* was polymerase chain reaction (PCR) – amplified and inserted between the 5'EcoRI and 3'XhoI restriction sites of the multiple cloning site in the pET23d (+) and pGEX4T3 vectors. The recombinant T7-Vac14-HIS protein contains a T7 epitope on the N-terminus and a 6xHIS tag on

the C-terminus. Both the T7 epitope and the 6xHIS tag can be used for affinity purification and Western blot detection with antibodies. The recombinant glutathione S-transferase-Vac14 (GST-Vac14) contains a GST tag on the N-terminus which can also be used for affinity purification and Western blot detection with antibodies.

The vector encoding T7-TEV-Vac14-HIS was generated by digestion of the T7-Vac14-HIS with EcoRI and re-ligating with an oligonucleotide adaptor encoding the Tobacco Etch Virus (TEV) peptide sequence (Glul-Asn-Leu-Tyr-Phe-Gln-Gly), which is cleaved by the GST-TEV-HIS protease between Gln and Gly (Eton Bioscience Inc.). The TEV oligonucleotides were generated by annealing the forward 5'*AATTC*GAGAAAACCTGTATTTTCAGGGCCG3' and complementary reverse 5'*AATTC*GGCCCTGAAAATACAGGTTTTCTCG3' oligonucleotide to generate double stranded oligonucleotide with 5' and 3' ends compatible with EcoRI (italics represents EcoRI restriction site overhangs). One unit of polynucleotide kinase was used to phosphorylate both 5' ends of the TEV oligonucleotides at 37°C for one hour and subsequently inactivated at 70°C for 20 min. Phosphorylated TEV oligonucleotides were then allowed to anneal to form double stranded DNA. The pET23d(+) vector containing coding sequence for T7-Vac14-HIS was treated with EcoRI restriction enzyme (NEB) at 37°C for 2 hours and alkaline phosphatase at 65°C for one hour. The digested products were purified using an EZ-10 Cleanup Kit (Bio-Basic Ltd.) as per manufacturers' instructions. The double stranded TEV oligonucleotide was then ligated into the digested pET23d(+) containing coding sequence for T7-Vac14-HIS using T4 DNA ligase (NEB) at 16°C overnight. Ligated products were transformed into DH5α and the plasmid DNA was subsequently purified from multiple colonies as previously described. Purified plasmid DNA (6 µl) were digested with EcoRI and XhoI restriction enzymes (NEB) that flanks the 5' and 3' ends of the coding sequence for Vac14 in the

pET23d(+) vector at 37°C for 2 hours. Digested products were resolved on 0.8% agarose gel with ethidium bromide and visualized under UV illumination to check for presence of T7-TEV-VAC14-HIS insert (~2.5kb) and vector (~3.5kb). Plasmid DNA containing the T7-TEV-VAC14-HIS insert was sent for sequencing at The Centre for Applied Genomics. The presence of correctly inserted TEV oligonucleotide in the pET23d(+) containing coding sequence for T7-Vac14-HIS was verified using the Geneious program. The plasmid, pCH1, containing coding sequence for T7-TEV-Vac14-HIS was then transformed into BL21(DE3) as previously described.

2.5 Expression and concentration of recombinant T7-Vac14-HIS

BL21 DE3 containing T7-Vac14-HIS expression vector was grown overnight at 37°C in LB media supplemented with 100 µg/ml ampicillin. Overnight culture was then added to 1L of Super Broth (SB) media with 100 µg/ml ampicillin to obtain an initial OD_{600} of 0.15. The culture was grown at 37°C with constant shaking to an OD_{600} of 0.6-0.8. Cultures were then grown overnight at 18°C for expression of recombinant T7-Vac14-HIS in the absence of IPTG due to leaky expression. Lysates were collected by centrifugation at 4000 rpm for 30 min at 4°C. The cell pellet was immediately resuspended in 20 ml of HIS-lysis buffer (50 mM Tris-HCl, pH 8.0, 300 mM NaCl, and 20 mM imidazole) supplemented with 0.5 mg/ml lysozyme, 30 mg/ml EDTA, 2 mM β-mercaptoethanol (BME), 10 mM Benzamide, 0.2 mM AEBSF, and bacterial protease cocktail A (Bio-basic Ltd.). Cells were lysed with lysozyme at 4°C for 2 hours with constant rotation and sonicated in an ice bath for 4 pulses of 15 s each (output 50) or using a French Press. Supernatant was collected by centrifugation at 4000 rpm for 30 min at 4°C.

To concentrate recombinant T7-Vac14-HIS, 500 µl of packed Ni^{2+}-NTA beads (Bio-basic Ltd.) were washed 4 times with 5 min washes of 1 ml HIS-lysis buffer with 2mM BME.

Washed Ni^{2+}-NTA beads were incubated in the supernatant at 4°C for 2 hours with constant rotation. Beads were then washed four times with 1 ml of HIS-lysis buffer with 2 mM BME at 4°C for 5 min each. Recombinant T7-Vac14-HIS was batched eluted by constant rotation at 4°C for 5 min with three 500 µl HIS-elution buffer (50 mM Tris-HCl, pH 8.0, 300 mM NaCl, and 250 mM imidazole) supplemented with 2 mM BME and pooled together. Purified recombinant T7-Vac14-HIS was dialyzed overnight in D-Tube Dialyzer Maxi (Novagen) with molecular weight cutoffs from 7-8 kDa at 4°C with dialysis buffer (50 mM Tris-HCl, pH 8.0, 200 mM NaCl) supplemented with 2 mM BME. Concentration of recombinant T7-Vac14-HIS was estimated by comparison with known concentration of bovine serum albumin (BSA) standard by coomassie blue stain. Aliquots of 60 µl of ~1-3 µg/µl recombinant T7-Vac14-HIS were flash-frozen with liquid nitrogen and stored at -80°C.

2.6 Tandem purification of T7-TEV-Vac14-HIS by affinity chromatography

Recombinant T7-TEV-Vac14-HIS was expressed in BL21 (DE3), lysed and concentrated as described previously for recombinant T7-Vac14-HIS. To purify recombinant T7-TEV-Vac14-HIS, 500 µL of agarose beads conjugated to anti-T7 antibodies (Novagen) were washed four times with 1 ml HIS-lysis buffer with 2 mM BME. Washed beads were then incubated with concentrated recombinant T7-TEV-Vac14-HIS obtained from Ni^{2+}-NTA affinity chromatography at 4°C for 2 hours with constant rotation. Beads were then washed four times with 1 ml of HIS-lysis buffer with 2 mM BME. Three microliters of 60 units of GST-TEV-HIS protease (Eton Bioscience Inc.) were added to the beads with 300 µl of dialysis buffer and incubated overnight at 4°C with constant rotation. The supernatant was then extracted and incubated with 3 times of 50 µl packed glutathione beads (GE Healthcare) that was previously washed with dialysis buffer, at 4°C for 2 hours, to isolate GST-TEV-HIS. Supernatant was

extracted and 10% of supernatant were resolved in 9% SDS-PAGE to verify purity of recombinant Vac14-HIS and to estimate concentration by comparison with known BSA standards. Samples were flash-frozen with liquid nitrogen and stored at -80°C.

2.7 Expression and purification of GST-fusion proteins for in-vitro binding assay

Overnight cultures of BL21 DE3 carrying the expression vector for GST-Vac14 or GST were grown as previously indicated. Induction of expression was achieved with the addition of 0.5 mM IPTG and grown for 4 hours at 30°C. Cell lysates were collected by centrifugation at 4000 rpm for 30 min at 4°C. Cell lysates were immediately resuspended in GST-lysis buffer (20 mM Tris-HCl, pH 7.5, 100 mM NaCl) supplemented with 0.5 mg/ml lysozyme, 30 mg/ml EDTA, 2 mM BME, 10 mM Benzamide, 0.2 mM AEBSF, and bacterial protease cocktail A (Bio-basic Ltd.). Cells were lysed and supernatant was collected as before.

For purification of recombinant GST-tagged proteins, 100 µl of packed glutathione-beads were washed 4 times with 5 min washes of 1 ml HIS-lysis buffer with 2mM BME. Beads were then incubated with supernatant at 4°C for 2 hours with constant rotation. Beads were then washed 4 times with 5 min washes of 1 ml GST buffer A (50 mM Tris-HCl, pH 7.5, 100 mM NaCl, 2 mM BME) at 4°C. GST-tagged proteins were eluted with 20 mM glutathione in GST buffer B (50 mM Tris-HCl, pH 8.0, 200 mM NaCl, 2 mM BME) adjusted to pH 8.0 with concentrated NaOH. Purified recombinant GST-tagged proteins were dialyzed overnight in D-Tube Dialyzer Maxi (Novagen) with molecular weight cutoffs from 7-8 kDa at 4°C with dialysis buffer. Concentration of recombinant GST-tagged proteins was estimated by comparison with known BSA standard. Aliquots were flash-frozen with liquid nitrogen and stored at -80°C.

For in-vitro interaction assay, 300 µg of recombinant GST-tagged proteins were first immobilized on 200 µl packed glutathione beads as previously described and 200 µg purified

recombinant T7-Vac14-HIS were then added and incubated at 4°C for 2 hours with constant rotation. Beads were washed four times with GST-buffer B with 0.05% Tween-20 at 4°C for 5 min each. Bound recombinant proteins were extracted with 2X sample buffer (100mM Tris, pH 6.8, 4% SDS, 10% glycerol, 1% bromopheno blue, and 10% 2-mercaptoethanol).

2.8 SDS-PAGE and Western blotting for detection of recombinant proteins

Bacterial lysates, protein fractions from differential velocity ultracentrifugation and fast protein liquid chromatography with size exclusion chromatography (FPLC-SEC), and molecular weight standards were mixed with 2X sample buffer and heated at 100°C for 5 min. Samples were vortexed for 10 min prior to loading onto a discontinuous polyacrylamide gel with 5% stacking and 9% separating gels, and submerged in 1X Tris/SDS running buffer (Bio-basic Ltd.). Proteins were separated by applying 130 Volts for 2 hours. Some gels were stained with Bio-safe Coomassie Brilliant Blue (Bio-RAD) and destained with ddH_2O or used unstained for Western blotting.

For Western blotting, proteins were transferred to a Polyvinylidene fluoride (PVDF) membrane (Pall Corporation) at 100 Volts for 1 hour in 1X Tris/Glycine transfer buffer (Bio-basic Ltd). Membranes were blocked in 1X Tris buffered saline (TBS) (20 mM Tris, 150 mM NaCl, 2 mM KCl, pH 7.4) plus 0.05% Tween-20 with 5% skim milk for one hour at ambient temperature prior to incubating with the primary antibody diluted into 15 ml (1 in 15,000 for mouse monoclonal α-T7 antibody) at 4°C overnight with constant gentle agitation. Unbound primary antibody was washed away 4X with 5 min washes in 15 ml 1X TBS-0.05% Tween-20 prior to incubating membrane with the secondary HRP-conjugated anti-mouse antibody (Cedarlane Laboratories Limited, Ontario, Canada) diluted into 15 ml (1 in 15,000) at ambient temperature for 1 hour with gentle agitation. The membrane was then washed 4X with 5 min

washes in 15 ml 1X TBS plus 0.05% Tween-20. Blots were then incubated in 1 ml Immun-Star WesternC Chemiluminescent solution (Bio-RAD) or 1 ml of ECL plus Western blotting dection system (GE Healthcare) for 5 min as described by the manufacturer. Blots were then wrapped in Saran Wrap and exposed to chemiluminescence film (GE Healthcare Ltd.) in a dark room for 30 sec to 3 min. The autoradiography film was developed using GBX developer and replenisher (Kodak, Rochester, NY, USA), and fixed using GBX fixer and replenisher (Kodak, Rochester, NY, USA).

2.9 Fast protein liquid chromatography (FPLC)

Two Sephacryl columns were employed: the S200 column with a fractionation range of 5kDa – 250kDa and the S300 column with a fractionation range of 10kDa – 1,500kDa (GE Healthcare). Four protein standards – phosphorylase b (~97kDa) (Sigma), catalase (~250kDa) (Sigma), ferritin (~440kDa) (Calbiochem), and thyroglobulin (~660kDa) (Sigma) – were used to indicate the elution volume that correspond to the molecular weight standards, while blue dextran (Sigma) was used to indicate the void volume of the S300 Sephacryl column. One hundred microliters of 3 µg/µl protein standards, blue dextran and purified recombinant T7Vac14HIS were injected onto the column and run sequentially, and 1 ml fractions were collected. The presence of protein standards in each fraction was detected by reading A_{280}. Recombinant T7-Vac14-HIS was concentrated with 10% Trichloroacetic acid (TCA) (see below) and detected using western blotting with anti-T7 antibody.

2.10 Differential velocity ultracentrifugation with glycerol gradient

Ten to forty percent glycerol solutions were prepared in dialysis buffer. Three discontinuous glycerol density gradients were prepared by gently overlaying 3 ml of 40%, 3 ml of 30%, 2 ml of 20%, and 2 ml of 10% glycerol solutions (from bottom to top) in three 11 ml

polyallomer tubes. The discontinuous glycerol gradients were then spun for 1 hour at 30,000 rpm using a floor-top ultracentrifuge (Optima L-100K, Beckman Coulter) to generate a continuous gradient. Four protein standards – phosphorylase b (~97.2kDa), catalase (~250kDa), ferritin (~440kDa), and thyroglobulin (~660kDa) – were used to indicate the density fractions that correspond to the molecular weight standards. One milliliter of samples containing 300 µg of protein standards (thyroglobulin with catalase and ferritin with phosphorylase b) and purified recombinant T7-Vac14-HIS were gently layered on top of three independent gradients. The three glycerol gradients containing protein samples were then centrifuged at 30,000 rpm for 5 hours at 4°C in a swinging bucket SW41 Ti rotor (Beckman Coulter). One millilitre fractions were then collected. Protein standards were detected by reading absorbance at 280 nm (A_{280}), while the recombinant T7-Vac14-HIS fractions were concentrated with 10% TCA (see below) and detected by Western blotting with anti-T7 antibody (Novagen).

2.11 Protein precipitation for Western blotting detection

Proteins from differential velocity ultracentrifugation with glycerol gradients and FPLC were precipitated with 10% (TCA) before analysis with Western blotting. 100X TCA (100 µl) was added to 1 ml sample and incubated on ice for 30 min. Precipitates were collected by centrifugation at 15,000 rpm for 30 min and washed with 2x 1 ml cold acetone, air dried and re-suspended in 100 µl 2X sample buffer.

3. Results

3.1 Optimization of recombinant T7-Vac14-HIS expression in BL21(DE3)

The pET23d+ vector containing the coding sequence for Vac14 was transformed into *E.coli* BL21(DE3). Different conditions, including induction time, temperature, and concentration of the inducer, IPTG, were tested to optimize the expression of recombinant T7-Vac14-HIS in *E.coli* BL21(DE3) (Table 3.1). The presence of recombinant T7-Vac14-HIS was detected using Western blot with anti-T7 antibodies (Figure 3.1). This enables the detection of full-length recombinant T7-Vac14-HIS and the N-terminal fragments, an indicator of degradation.

To identify the optimum induction time, *E.coli* BL21(DE3) transformed with vector for recombinant T7-Vac14-HIS was exposed to 0.5mM IPTG at 30°C for a durations of 2, 3, 4, 5 and 6 hours (Table 3.1A and Figure 3.1A). *E.coli* BL21(DE3) without vector was used as a negative control, demonstrating that bacterial proteins without the T7-epitope do not have affinity for anti-T7 antibodies (Figure 3.1A lane 1). The level of expression of full-length recombinant T7-Vac14-HIS, indicated by the band at ~100kDa, is relatively the same with different durations of induction time (Table 3.1A and Figure 3.1A lanes 2-6).

A second negative control was used to indicate the absence of recombinant T7-Vac14-HIS when the transformed *E.coli* BL21(DE3) is not induced (Figure 3.1A lane 7). Surprisingly, recombinant T7-Vac14-HIS and its degraded products were detected due to leaky expression. Another interesting finding is that, the un-induced sample appears to have less degraded products compared to the induced samples, while the level of full-length recombinant T7-Vac14-HIS remains relatively the same (Figure 3.1A).

To test for the effect of IPTG, different concentration of IPTG were tested to optimize expression of the full-length recombinant T7-Vac14-HIS. Increasing concentration of IPTG did not increase the level of expression of full-length recombinant T7-Vac14-HIS but instead increased the level of degraded products of the recombinant T7-Vac14-HIS (Table 3.1B). In agreement with the previous experiment testing for optimal induction time, full-length recombinant T7-Vac14-HIS was found in the control that was not induced with IPTG (Figure not shown). The un-induced sample has similar level of full-length recombinant T7-Vac14-HIS, but less degraded products compared with the induced sample (Table 3.1B). Thus, zero IPTG has best expression of full-length recombinant T7-Vac14-HIS and minimal degraded products.

To test for optimal induction temperature, recombinant T7-Vac14-HIS was expressed in the absence of IPTG at different temperature. Due to the slower growth of bacteria at low temperature, such as 18°C, recombinant T7-Vac14-HIS was expressed overnight. While the expression of recombinant T7-Vac14-HIS was expressed at 37°C, 30°C, 26°C, and 22°C for 4 hours (Figure 3.1B). Both the level of expression for full-length T7-Vac14-HIS and the degraded products are relatively the same at 37°C, 30°C, 26°C, and 22°C (Figure 3.1B lanes 2-5). In comparison, the level of expression of full-length recombinant T7-Vac14-HIS at 18°C was almost double the level observed at 37°C, 30°C, 26°C, and 22°C (Table 3.1C and Figure 3.1B lane 1). In addition, the level of degraded products is also at its minimum when expressed at 18°C overnight (Figure 3.1B lane 1). Thus, recombinant T7-Vac14-HIS is best expressed overnight at 18°C without the addition of IPTG.

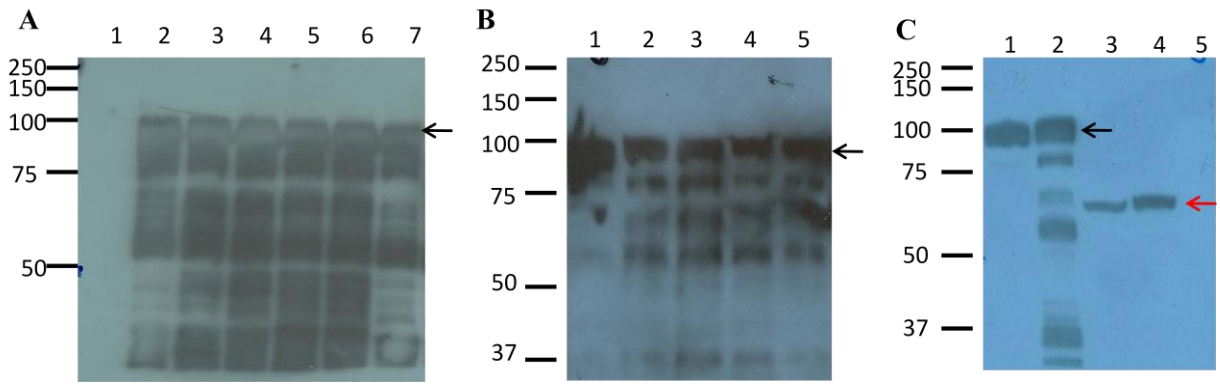

Figure 3.1. Western blots with anti-T7 antibody of whole cell lysates for the presence of recombinant proteins. Molecular protein standards are indicated in all figures. Monomeric recombinant T7-Vac14-HIS (~100kDa) indicated with a black arrow. Monomeric recombinant T7-fig4-HIS (~74kDa), a Fig4 truncation, indicated with a red arrow. (A) BL21(DE3) with no plasmid (lane 1). Expression of T7-Vac14-HIS in 0.5mM IPTG at 30°C for 2, 3, 4, 5, and 6 hours (lanes 2-6, respectively). Uninduced BL21(DE3) transformed with T7-Vac14-HIS plasmid at 30°C for 5 hours (lane 7). (B) Expression of recombinant T7-Vac14-HIS at 18°C overnight (lane 1) and 22°C, 26°C, 30°C, and 37°C for 4 hours in the absent of IPTG. (lanes 2-5, respectively). (C) Expression of recombinant T7-Vac14-HIS at 18°C overnight with and without IPTG (lanes 1-2, respectively). Expression of recombinant truncated T7-fig4-HIS overnight with and without IPTG (lanes 3-4, respectively. BL21(DE3) with no plasmid (lane 5).

Table 3.1 Optimized induction time, concentration of IPTG, and temperature for expression of recombinant T7-Vac14-HIS.

A

Time (hr)	2	3	4	5	6
T7-Vac14-HIS	++	++	++	++	++
Degraded products	++	+++	+++	+++	+++

B

[IPTG]	0 mM	0.25 mM	0.5 mM	0.75 mM	1 mM
T7-Vac14-HIS	++	++	++	++	++
Degraded products	++	+++	+++	++++	++++

C

Temperature	18 °C	22 °C	26 °C	30 °C	37 °C
T7-Vac14-HIS	++++	++	++	++	++
Degraded products	+	++	++	++	++

Recombinant T7-Vac14-HIS was expressed in *E.coli* BL21(DE3). The relative level of full-length recombinant T7-Vac14-HIS and degraded products are indicated as '+'. (A) Expression of recombinant T7-Vac14-HIS with 0.5 mM IPTG at 30 °C for 2, 3, 4, 5, and 6 hours. (B) Expression of recombinant T7-Vac14-HIS at 30°C for 4 hours with different concentration of IPTG (0, 0.25, 0.5, 0.75 and 1mM). (C) Expression of recombinant T7-Vac14-HIS with no IPTG for 4 hours at 22°C, 26°C, 30°C, 37°C, and at 18°C for overnight.

3.2 Concentration of recombinant T7-Vac14-HIS with Ni^{2+}-affinity chromatography

Purified soluble recombinant T7-Vac14-HIS is needed for the identification of the multimeric state of recombinant T7-Vac14-HIS. To purify recombinant T7-Vac14-HIS, transformed BL21(DE3) was lysed by French Press and lysozyme treatment. Recombinant T7-Vac14-HIS was found in both soluble and insoluble fractions after cell lysis with the French Press (Figure 3.2A lane 3 and 4). The soluble recombinant T7-Vac14-HIS was concentrated by Ni^{2+}-NTA agarose affinity chromatography (Figure 3.2A lane 5; figure 3.2B lane 2). The concentrated sample contains the full-length recombinant T7-Vac14-HIS indicated by the protein band at ~100kDa (black arrow) in both Coomassie brilliant blue stain and Western blot with anti-T7 antibodies (Figure 3.2A lane 5; figure 3.2B lane 2). Proteins found below the ~100kDa full-length recombinant T7-Vac14-HIS could possibly be degraded products of recombinant T7-Vac14-HIS containing the C-terminal 6xHIS tag that were also purified by Ni^{2+}-NTA agarose (Figure 3.2B lane 2*). Another possibility is that, native bacterial proteins might also display affinity for Ni^{2+}-NTA agarose. Full-length recombinant T7-Vac14-HIS was found to be ~2-3 µg/µl by comparing to BSA standards (Figure 3.2B lane 3-4) (see T7-TEV-Vac14-HIS section for a procedure to eliminate remaining impurities).

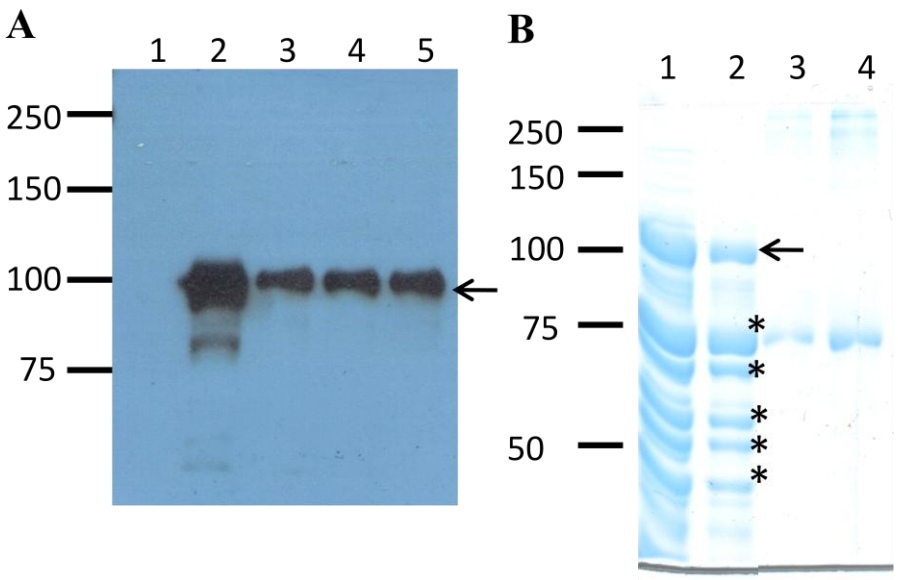

Figure 3.2. Concentrated recombinant T7-Vac14-HIS by Ni^{2+}-affinity chromatography. Molecular protein standards are indicated in all figures. (A) Western blot with anti-T7 antibody for recombinant T7-Vac14-HIS. Whole cell lysate of BL21(DE3) without plasmid (lane 1). Expression of recombinant T7-Vac14-HIS at 18°C overnight in the absence of IPTG (lane 2). Insoluble and soluble recombinant T7-Vac14-HIS (lane 3 and 4, respectively). Soluble recombinant T7-Vac14-HIS (lane 5). (B) Coomassie stain for quantification of recombinant T7-Vac14-HIS expression in BL21(DE3) at 18°C overnight with no IPTG. Whole cell lysate (lane 1), purification with Ni^{2+}-NTA beads (lane 2). Monomeric recombinant T7-Vac14-HIS (~100kDa) (black arrow). Likely example of degraded products containing the C-terminal 6xHIS tag (*). 10µg and 20µg BSA were used to estimate the concentration of recombinant T7-Vac14-HIS (lane 3-4, respectively).

3.3 In-vitro recombinant Vac14 self-interaction

To confirm recombinant Vac14 was functional and to replicate results by Botelho et al. [6], Vac14 self-interaction was assayed in-vitro using recombinant T7-Vac14-His and GST-Vac14 (Figure 3.3). Purified recombinant T7-Vac14-His was incubated with GST or GST-Vac14 coated glutathione beads. The GST coupled to glutathione beads was not able to pull down recombinant T7-Vac14-His, indicating that there was no non-specific binding between GST and the beads with recombinant T7-Vac14-His. In comparison, GST-Vac14 coupled to glutathione beads was able to pull down recombinant T7-Vac14-His, but the interaction was relatively weak compared to the input (Figure 3.3). However, the weak signal observed for the interaction between recombinant T7-Vac14-His and GST-Vac14 could be due to the presence of competing T7-Vac14-His to T7-Vac14-HIS or GST-Vac14 to GST-Vac14 self interactions.

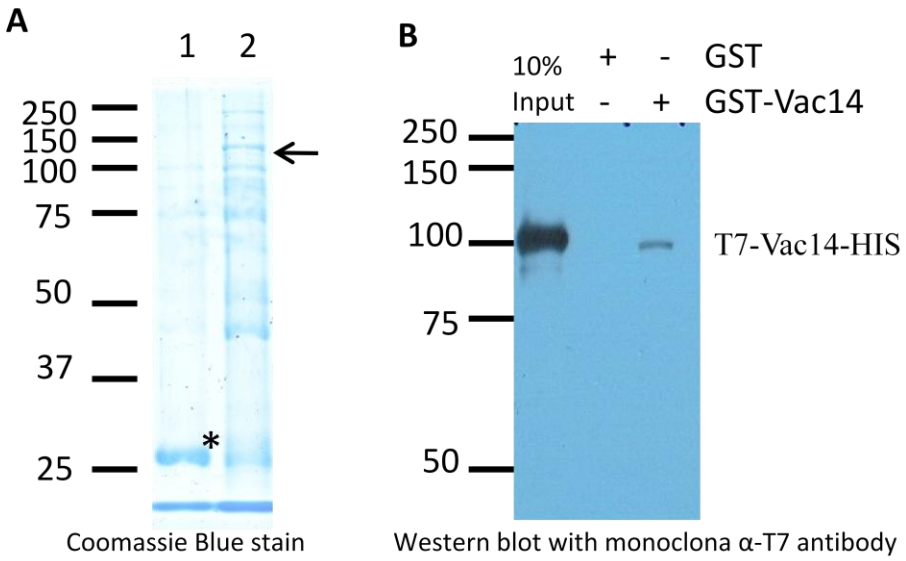

Figure 3.3. In-vitro Vac14 self-interaction. Molecular protein standards are indicated in all figures. (A) GST (*) and GST-Vac14 (black arrow) was purified using glutathione-Sepharose beads (lane 1-2, respectively). (B) Purified GST and GST-Vac14 coated on glutathione-Sepharose beads were incubated with purified recombinant T7-Vac14-HIS. Input lane represents 10% of the total purified recombinant T7-Vac14-HIS used. Remaining lanes represent total bound proteins detected by western blot with α-T7 antibodies.

3.4 Fast protein liquid chromatography using size-exclusion chromatography to identify the molecular weight of recombinant T7-Vac14-HIS multimer

To begin identifying the multimeric state of recombinant T7-Vac14-HIS, an ÄKTA FPLC system with a Sephacryl S200 size-exclusion column was used. The ÄKTA FPLC is an automated system that injects a sample of macromolecules for analysis while pumping the solvent through the column at a constant flow rate. As the macromolecules migrate through the size-exclusion column, which has a fractionation range of 5 – 250 kDa, the macromolecules will elute out of the column according to the molecular weight and shape of the individual macromolecule. Three molecular weight standards were used: phosphorylase b (~97 kDa), catalase (~250 kDa) and thyroglobulin (~660 kDa). As the individual protein standard elutes out of the size-exclusion column, the presence of the proteins is detected at 280 nm and recorded as a function of elution volume (Figure 3.4A). The FPLC system also collects the elution in 1 ml fractions for future analysis.

A mixture of thyroglobulin and phosphorylase b was first injected into the size-exclusion column. Elution of phosphorylase b peaked at ~50.4 ml (Figure 3.4A). Catalase was also injected into the size-exclusion column in a mixture containing thyroglobulin. Elution of catalase (~250 kDa) started at ~42 ml, peaked at ~46 ml and ended at ~48 ml (Figure 3.4A). Elution of thyroglobulin peaked at ~38 ml (Figure 3.4A). Due to the molecular weight of thyroglobulin (~660 kDa) is higher than the upper range of the fractionation range of ~250 kDa, proteins that also elutes at ~38 ml of the Sephacryl S200 size-exclusion column are considered to be in the void volume.

After injection of purified recombinant T7-Vac14-HIS, 1 ml elution fractions were collected and analyzed by Western blot using anti-T7 antibodies for the presence of recombinant

T7-Vac14-HIS. Monomeric recombinant T7-Vac14-HIS has a molecular weight of ~100 kDa, which is similar to the molecular weight of phosphorylase b, ~97 kDa. However, recombinant T7-Vac14-HIS was not detected in the elution volume that corresponds to phosphorylse b at ~50.4 ml (Figure 3.4B blue arrow). If recombinant T7-Vac14-HIS is found within the catalase elution curve, it would suggest that recombinant T7-Vac14-HIS mutlimer exists as a dimer (~200 kDa) or a trimer (~300 kDa). However, recombinant T7-Vac14-HIS was not detected anywhere within elution curve for catalase (Figure 3.4B red arrow). Purified recombinant T7-Vac14-HIS was found in ~38 ml elution fraction that corresponds to thyroglobuin (Figure 3.4B purple arrow). This suggests that recombinant T7-Vac14-HIS exists as a multimer that has a molecular weight greater than 250 kDa. However, because FPLC size-exclusion is affected by the Stoke's radius of the macromolecule, the Stoke's radius of the recombinant T7-Vac14-HIS may affect its rate of migration through the size-exclusion column.

Since the results with the FPLC Sephacryl S200 size-exclusion column were not conclusive, we opted to use the Sephacryl S300 size-exclusion column that has a higher fractionation range of 10 – 1,500 kDa. Four molecular weight standards (thyroglobulin, ferritin (~440 kDa), catalase, and phosphorylase b) were used to relate the elution volume with molecular weight, while blue dextran, a polymer that has a molecular weight of ~2,000 kDa was used to identify the void volume (Figure 3.5A). The results from the Sephacryl S300 again indicated that the recombinant T7-Vac14-HIS multimer eluted in the void volume along with the blue dextran (Figure 3.5B blue arrow). The result from FPLC Sephacryl S300 size-exclusion column fractionation was again inconclusive, suggesting either the recombinant T7-Vac14-HIS multimer has a molecular weight that is greater than 1,500 kDa or the Stoke's radius of the

recombinant T7-Vac14-HIS multimer is affecting its migration through the column causing the multimer to behave as if it is greater than 1,500kDa.

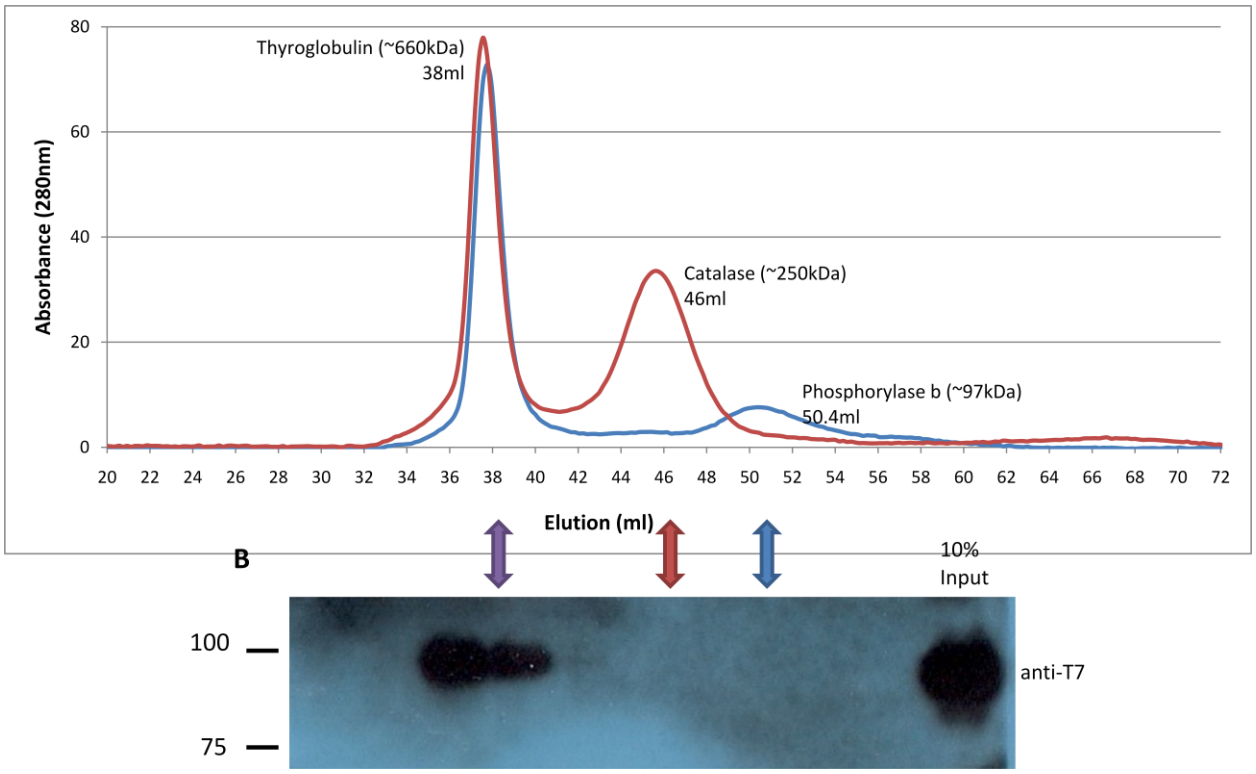

Figure 3.4. Identification of the molecular weight of recombinant T7-Vac14-HIS multimer by gel fractionation with Sephacryl S200 column. (A) One hundred microliter of 3 mg/ml of each protein standard were injected into the ÄKTA FPLC connected to a Sephacryl S200 column. Elution of protein standards (phosphorylase b, catalase, and thyroglobulin) was detected by absorbance reading at 280 nm. (B) One hundred microliters of 3 mg/ml purified recombinant T7-Vac14-HIS was injected into the ÄKTA FPLC connected to a Sephacryl S200 column and collected in 1 ml fractions. Recombinant T7-Vac14-HIS was detected by Western blot using anti-T7 antibodies. Input lane represents 10% of the total recombinant T7-Vac14-HIS injected onto the S200 column. The elution volume that relates to thyroglobulin is at 38 ml (purple arrow), the elution volume that relates to catalase is at 46 ml "red arrow", and the elution volume that relates to phosphorylase b is at 50.4 ml "blue arrow".

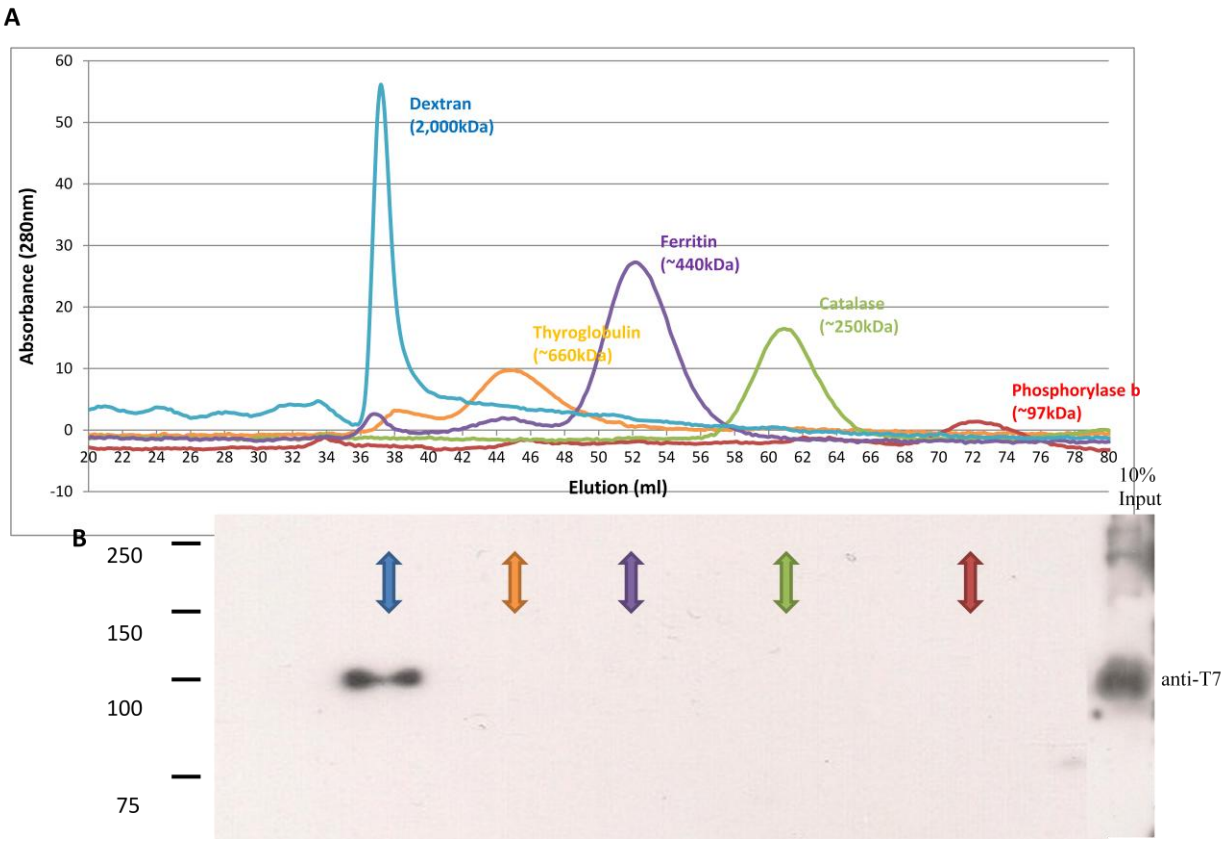

Figure 3.5. Identification of the apparent molecular weight of recombinant T7-Vac14-HIS multimer with gel filtration by Sephacryl S300 column. (A) One hundred microliters of 3 mg/ml of each protein standards were injected onto the S300 column. Elution of protein standards (Dextran, thyroglobulin, ferritin, catalase, and phosphorylase b) were detected by absorbance reading at 280 nm. (B) One hundred microliters of 3 mg/ml purified recombinant T7-Vac14-HIS was injected into the ÄKTA FPLC Sephacryl S300 column and were collected in 1 ml fractions. Recombinant T7-Vac14-HIS was detected by Western blot using anti-T7 antibodies. Input lane represents 10% of the total recombinant T7-Vac14-HIS injected onto the S300 column. Elution volume that relates to Dextran, thyroglobulin, ferritin, catalase, and phosphorylase b are indicated by "blue", "orange", "purple", "green", and "red" arrows, respectively.

3.5 Differential velocity ultracentrifugation with a glycerol gradient to estimate the molecular weight of the recombinant T7-Vac14-HIS multimer

An alternative method was needed for identifying the apparent molecular weight of recombinant T7-Vac14-HIS multimer due to the inconclusive results from gel filtration with size-exclusion chromatography. Differential velocity ultracentrifugation through a glycerol gradient separates macromolecules according to their molecular weight and is not significantly affected by the Stoke's radius of macromolecules [7, 53]. Thus, differential velocity ultracentrifugation with a 10-40% glycerol gradient was also used to identify the molecular weight of the recombinant T7-Vac14-HIS multimer.

After ultracentrifugation of individual molecular weight standards and recombinant T7-Vac14-HIS in the 10-40% glycerol gradients, 1 ml fractions were collected for analysis. Absorption at 280 nm was used to identify glycerol fractions that contained the four molecular weight standards (phosphorylase b, catalase, ferritin, and thyroglobulin). Heavier molecular weight standards migrated further into the denser glycerol gradients. Phosphorylase b was concentrated in fraction 1, catalase in fraction 2, ferritin in fraction 5 and thyroglobulin in fraction 9 (Figure 3.6A). The presence of recombinant T7-Vac14-HIS in the glycerol fractions were analyzed by Western blot with anti-T7 antibodies. Recombinant T7-Vac14-HIS was found in fractions 1 to 4, with a peak between fractions 2-3 (Figure 3.6B). There is a weak signal of recombinant T7-Vac14-HIS in fraction 1, which corresponds to phosphorylase b that has a molecular weight of ~97 kDa (Figure 3.6B blue arrow). This suggests that there are minimal traces of monomeric recombinant T7-Vac14-HIS (~100 kDa) in the purified sample. The recombinant T7-Vac14-HIS peaks at fractions 2 and 3, which corresponds to catalase (Figure 3.6B green arrow). This suggests that recombinant T7-Vac14-HIS multimer could be a dimer

(~200 kDa) and/or a trimer (~300 kDa) because traces of recombinant T7-Vac14-HIS are also found in fraction 4 (Figure 3.6B). Recombinant T7-Vac14-HIS was not found in later fractions that correspond to ferritin and thyroglobulin (Figure 3.6B red and purple arrows). This suggests that the multimeric state of recombinant T7-Vac14-HIS multimer is not greater than a trimer. These results suggest that FPLC fractionation pattern is due to a large Stoke's radius and that the differential velocity ultracentrifugation with glycerol gradient is a better test for estimating the multimeric state of recombinant T7-Vac14-HIS multimer.

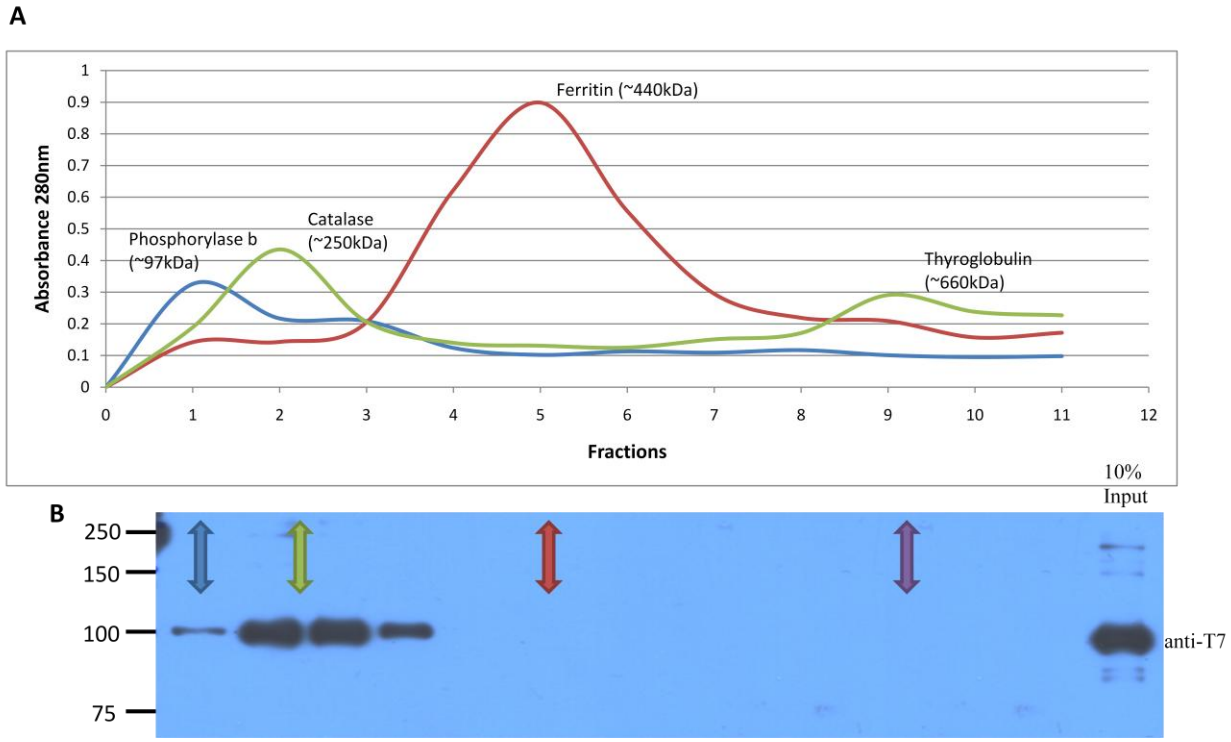

Figure 3.6. Identification of the molecular weight of recombinant T7-Vac14-HIS multimer with differential velocity ultracentrifugation in a 10-40% glycerol gradient. Approximately 300 µg of each protein standards and purified recombinant T7-Vac14-HIS were layered onto individual glycerol gradients and centrifuged at 30,000 rpm for 5 hours. Glycerol gradients were collected in 1 ml fractions (A) detection of molecular weight standards with absorbance readings at 280 nm. (B) detection of recombinant T7-Vac14-HIS with Western blot using anti-T7 antibodies. Input lane represents 10% of the total recombinant T7-Vac14-HIS layered onto the glycerol gradient. Fractions corresponding to the molecular weight standards, phosphorylase b, catalase, ferritin, and thyroglobulin are indicated with "blue", "green", "red", and "purple" arrows, respectively.

3.6 Tandem purification of recombinant T7-Vac14-HIS

A third method, analytical ultracentrifugation, will be used to support the result obtained from differential velocity ultracentrifugation with a glycerol gradient. However, a homogenous recombinant Vac14 will be required for analytical ultracentrifugation analysis. Therefore, the concentrated recombinant T7-Vac14-HIS was subjected to further purification to eliminate degraded products (Figure 3.7 lane 1). Full-length recombinant T7-Vac14-HIS was successfully isolated by anti-T7 antibody conjugated to agarose beads from the degraded products (Figure 3.7 lane 2). We then tried to use the T7 peptide to elute the full-length recombinant T7-Vac14-HIS by competition for interaction with anti-T7 antibody conjugated to agarose beads. However, after several trials of overnight elution with 1 mg/ml T7 peptide, full-length recombinant T7-Vac14-HIS remained bound to the anti-T7 antibody conjugated to agarose beads (Figure 3.7 lane 3). This suggest that the dissociation constant of anti-T7 antibody for T7 epitope is very low, such that excess amounts of T7 peptide could not display the bound recombinant T7-Vac14-HIS. A new method to release the bound recombinant T7-Vac14-HIS was then devised.

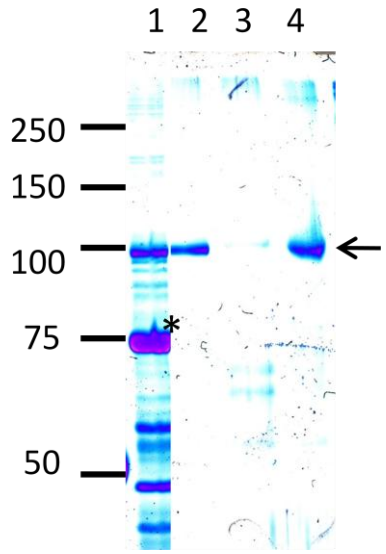

Figure 3.7. Coomassie stain to detect recombinant T7-Vac14-HIS purified with anti-T7 antibody conjugated to agarose beads. Molecular weight standards are indicated. Recombinant T7-Vac14-HIS purified with Ni^{2+}-NTA (Lane 1). Recombinant T7-Vac14-HIS bound to anti-T7 agarose after Ni^{2+}-NTA (Lane 2). Elution of recombinant T7-Vac14-HIS with 1 mg/ml T7 peptide (Lane 3). Recombinant T7-Vac14-HIS that remained bound to anti-T7 agarose after elution (Lane 4).

3.7 Cloning of T7-TEV-VAC14-HIS

An oligonucleotide adaptor encoding the peptide region recognized by TEV protease was generated by annealing the forward and reverse oligonucleotides. The oligonucleotide adaptor was designed to contain a 5' and 3' EcoRI sites that were used for ligation into to the EcoRI digested pET23d(+) vector containing the coding sequence for T7-Vac14-HIS between the sequence for T7 and VAC14 (Figure 3.8). Sequence alignment confirmed that the TEV recognized peptide was cloned in-frame between the N-terminal T7 epitope and Vac14 (Figure 3.9).

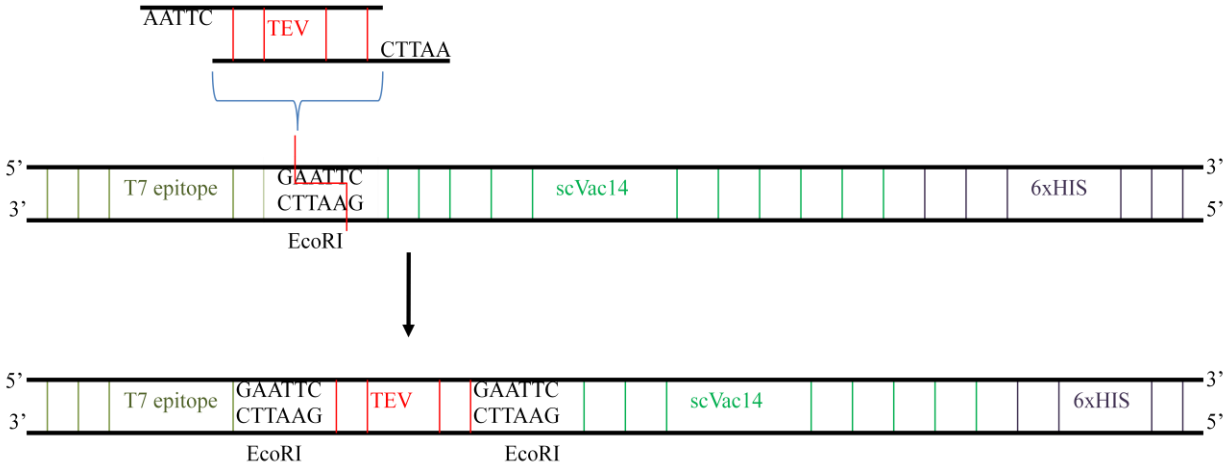

Figure 3.8 Cloning strategy for recombinant T7-TEV-VAC14-HIS. The oligonucleotide sequence coding for the TEV protease recognition site was designed to contain a 5' and 3' EcoRI site overhang. The double stranded oligonucleotide sequence was inserted into the EcoRI site between the coding sequence for the T7 epitope and Vac14, generating the coding sequence to express recombinant T7-TEV-Vac14-HIS.

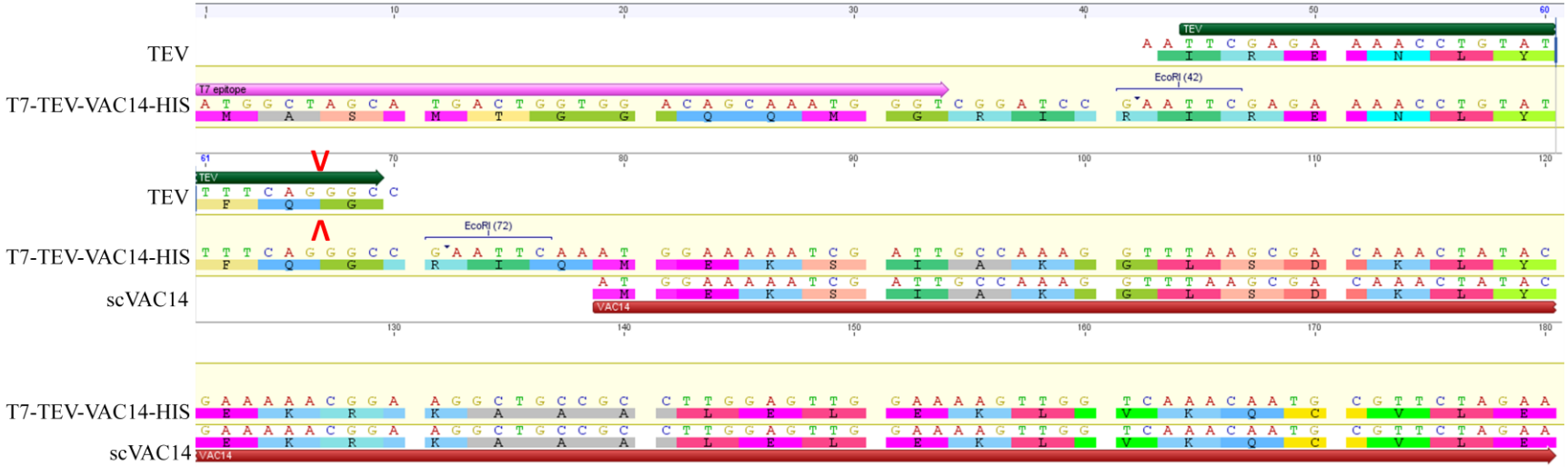

Figure 3.9 Sequence alignment of the initial section of T7-TEV-VAC14-HIS and the TEV cleavage site. The coding sequence for the T7 peptide within the T7-TEV-Vac14-HIS (Pink bar). The TEV oligonucleotide region recognized by the TEV protease is located between the T7-peptide sequence (Green bar) and the coding sequence of Vac14 (Red bar). The TEV protease cleaves between the Gln-Gly site (v).

3.8 Expression of T7-TEV-Vac14-HIS

The T7-TEV-Vac14-HIS was expressed in BL21(DE3) and concentrated by Ni^{2+}-affinity chromatography (Figure 5.3A). Concentrated sample of T7-TEV-Vac14-HIS also contains degraded products of less than 100 kDa (Figure 5.3A). Full-length recombinant T7-TEV-Vac14-HIS will be purified using anti-T7 antibody conjugated to agarose beads and subsequently cleaved by GST-TEV-HIS to elute recombinant Vac14-HIS for analytical ultracentrifugation analysis (see Future Directions).

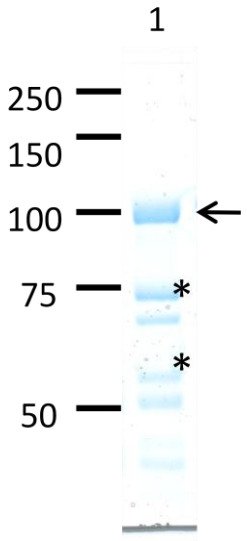

Figure 3.10 Concentration of T7-TEV-Vac14-HIS. BL12(DE3) was transformed with a vector containing coding sequence for T7-TEV-Vac14-HIS. Recombinant T7-TEV-Vac14-HIS was expressed overnight at 18°C without the addition of IPTG. Molecular weight markers are indicated. Concentrated T7-TEV-Vac14-HIS with Ni^{2+}-affinity chromatography for the 6xHIS C-terminal epitope (lane 1). Degraded products (*).

4. Discussion

PtdInsPs are important signalling molecules because their presence on specific organelles orchestrates organelle identity by binding and recruiting effector proteins to organelle membrane. Recent findings indicate the importance of PtdIns(3,5)P_2 in various pathways including the regulation of Ca^{2+} channels, the morphology of late endolysosomal structures, and autophagy [38]. PtdIns(3,5)P_2 dysfunction is also believed to be linked to several human neurophathologies, such as Charcot-Marie-Tooth Diesease (CMT) and amyotrophic lateral sclerosis (ALS) [12, 13, 85, 86]. However, little is known about the regulation of PtdIns(3,5)P_2 and the downstream events that PtdIns(3,5)P_2 orchestrates. Although the main components involved in the synthesis of PtdIns(3,5)P_2 are known, the Fab1 kinase, the Fig4 phosphatase, and the Vac14 regulator, it is still a mystery of how these individual components fit together for the regulation of PtdIns(3,5)P_2. In order to help understand the regulation of PtdIns(3,5)P_2, we aimed to identify the multimeric state of Vac14, the core protein that regulates and holds the Fab1 kinase and Fig4 phosphatase together.

Previous studies showed that the mammalian and yeast Vac14 self-interacted to form a multimer. In mammals, it is suggested that ArPIKfyve forms a dimer or trimer. However, these studies did not take into account the possibility of potential Vac14 interactions with PIKfyve, Fig4 phosphatase, or other proteins. Here, we strive to identify the multimeric state of Vac14 in the absence of other potential Vac14 interactions by using recombinant Vac14. In this study, we propose that the putative multimeric state of recombinant T7-Vac14-HIS to be indeed a combination of homodimer and/or homotrimer.

4.1 Expression of recombinant T7-Vac14-HIS

In this study, the lac operon and the T7 promoter was used for the expression of recombinant T7-Vac14-HIS. It was found that the leaky expression of the lac operon offered optimum expression of recombinant T7-Vac14-HIS while minimizing degradation as detectable by Western blotting with α-T7 antibodies (Figure 3.1). In nature, the lac operon is used for the metabolism of lactose in the absence of glucose. The lac operon repressor, which is constitutively expressed by the lacI gene, binds to the lac operator when glucose is available in the environment. This inhibits the production of lactose permease, β-galactosidase, and transacetylase for effective transport of lactose into the cell and its digestion into glucose and galactose [3]. The presence of lactose or its analogs, binds to the repressor allowing the transcription of lactose permease, β-galactosidase, and transacetylase or recombinant protein that is cloned downstream of the lac operator. However, this system is known to have leaky expression. The lac operon has a basal expression because the lac repressor does not bind to the lac operator with 100% efficiency [3]. This allows the cell to continually transport lactose into the cell to adapt to a rapid change in environment and to avoid starvation [3]. As a result, there is leaky expression when the lac operon is used for the control of recombinant protein expression. The leaky expression by the lac operon is generally negligible, but in this study, a strong promoter, the T7 promoter, was used in conjunction with the lac operon. The T7 RNA polymerase of bacteriophage T7 is known to be highly selective and efficient at recognizing the T7 promoter for high level expression [76]. As a result, traces of the T7 polymerase from leaky expression were enough for optimal production of the recombinant T7-Vac14-HIS. Induced expression with IPTG can overwhelm the folding machinery generating improperly folded proteins and degradation.

4.2 Recombinant T7-Vac14-HIS in-vitro binding assay

Recombinant T7-Vac14-HIS was pulled down by GST-Vac14, demonstrating the ability of recombinant T7-Vac14-HIS to self-interact to form a multimer (Figure 3.3B). However, the signal at ~100 kDa corresponding to recombinant T7-Vac14-HIS was relatively weak compared to the 10% input (Figure 3.3B). There are a few potential reasons for the observed weak signal. First, the self-interaction between recombinant GST-Vac14 and T7-Vac14-HIS could be weak. Second, the sample of purified recombinant T7-Vac14-HIS also contains its degraded products (Figure 3.2B lane 2). This degraded form of recombinant T7-Vac14-HIS is believed to contain only the C-terminal end, and not the N-terminal due to the lack of detection by Western blot for the N-terminal T7-epitope with anti-T7 antibodies (Figure 3.2A). Previous studies with truncated mammalian Vac14 suggested that the C-terminal domain of Vac14 is responsible for Vac14 self-interaction. Thus, the recombinant GST-Vac14 can potentially be saturated with a combination of the full-length recombinant T7-Vac14-HIS and the degraded C-terminal form, which would not be detected by the Western blot using anti-T7 antibodies. Third, there is likely competing interaction between recombinant T7-Vac14-HIS with T7-Vac14-HIS, and GST-Vac14 with GST-Vac14, as well as T7-Vac14-HIS with GST-Vac14. In the present in-vitro studies, only the interaction between recombinant GST-Vac14 and T7-Vac14-HIS are detected. And finally, there is also the possibility that all these factors together contribute to the apparent “weak” interaction between recombinant Vac14. However, we do not believe there is weak interaction between Vac14-Vac14 because of the result obtained from differential velocity ultracentrifugation with glycerol gradient indicated by monomeric Vac14.

4.3 Fast protein liquid chromatography with size-exclusion chromatography

To determine the multimeric state of recombinant T7-Vac14-HIS, FPLC-SEC was used to identify the molecular weight of the purified recombinant T7-Vac14-HIS. In FPLC-SEC, a constant pressure is applied to the dissolved macromolecules as they flow through a column packed with porous matrix. The probability of the macromolecule to enter the porous gel is inversely proportional to the molecular weight of the macromolecule. The molecular weight will then be used to deduce the multimeric state of recombinant T7-Vac14-HIS. However, the results obtained from FPLC-SEC with both the Sephacryl S200 and Sephacryl S300 were inconclusive, since recombinant T7-Vac14-HIS eluted in the void volume of both the Sephacryl S200 and S300 (Figure 3.4 and 3.5). The result is consistent with previous data obtained by R.Botelho with endogenous Vac14-HA expression in *fab1Δfig4Δ* yeast double-mutants, a yeast strain deleted for two known Vac14 associated partners (unpublished). The majority of Vac14-HA was also found in the void volume of FPLC-SEC with Sephacryl S300 (Figure 4.1A) (unpublished). Data with the yeast system could be debatable due to presence of other potential partners. However, because recombinant T7-Vac14-HIS is expressed in a bacterial system, it is assumed that bacterial proteins have no influence on the recombinant T7-Vac14-HIS homomeric complex. Therefore, there are two possible explanations for the results obtained from FPLC-SEC. The recombinant T7-Vac14-HIS homomeric complex could be composed of greater than 10 copies of the monomer recombinant T7-Vac14-HIS (~100 kDa) generating a complex with a molecular weight that is greater than the upper range of the fractionation range of 1,500 kDa of the Sephacryl S300 column.

Perhaps a more plausible explanation is that, fractionation of the recombinant T7-Vac14-HIS is affected by the Stoke's radius of the multimeric complex. Many macromolecules are not

spherical but as they travel through a solution, they take on a hypothetical sphere like shape. The Stoke's radius (or the hydrodynamic radius) is essentially the radius of this apparent sphere, which is dependent on the molecular weight, shape and the volume that the macromolecule occupies in solution [10]. Thus, macromolecules that have elongated shapes in solution will be fractionated according to the Stoke's radius, which is translated into the apparent molecular weight of the macromolecule in solution, and not be fractionated according to its actual molecular weight. Sequence analyses of both mammalian and yeast Vac14 indicated it to be comprised of multiple HEAT repeats [23, 45]. A HEAT repeat is a conserved helix-loop-helix motif known to mediate protein-protein interactions (Figure 1.5A) [1]. Although the structure of the Vac14 has yet to be elucidated, other mammalian proteins containing multiple HEAT repeats are known to form a superhelical structure that may resemble an arch [34]. For example, the PR65/A subunit of the protein phosphatase 2A that contains 15 HEAT-repeats and importin β that has 17 HEAT-repeats both form a superhelical structure (Figure 1.5B and C) [35, 80]. The HEAT-repeat motifs found in recombinant T7-Vac14-HIS may assembles to form a superhelical structure, and when in solution, it may acquire a large Stoke's radius that is not reflective of the actual molecular weight of recombinant T7-Vac14-HIS. As a consequence, differential velocity ultracentrifugation with a glycerol gradient, which is less dependent on the shape of the molecule was used for determining the apparent molecular weight of recombinant T7-Vac14-HIS.

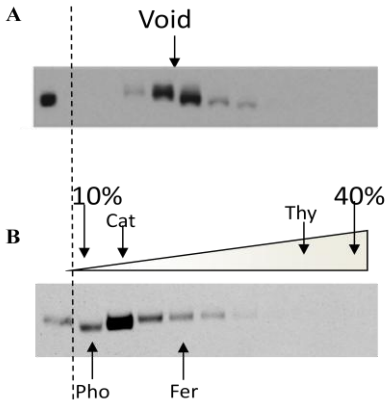

Figure 4.1 Identifying the molecular weight of yeast Vac14-HA. Vac14-HA expressed in *fab1Δfig4Δ* yeast double-mutants. FPLC-SEC Sephacryl S300 was used to estimate molecular weight of Vac14-HA (A). Differential velocity ultracentrifugation with a 10-40% glycerol gradients of the S100-membrane fraction containing vacuoles to identify the molecular weight of Vac14-HA (B). Pho: phosphorylate b; Cat: catalase; Fer: ferritin; Thy: thyroglobulin.

4.4 Differential velocity ultracentrifugation through a glycerol gradient

Ultracentrifugation with density gradients, such as the glycerol gradient used in this study, is based on the premise that when a constant centrifugal force is applied on a macromolecule, the different density of the glycerol exerts an increasing frictional force on the macromolecule as it migrates through the solution [53]. The distance that is covered by the macromolecule within a certain time frame is dependent largely on the molecular weight of the macromolecule [53]. However, due to the low resolution of the glycerol gradient, it cannot be used to pinpoint the exact distance the macromolecule travells, but instead gives a range of distance and a peak that it is most concentrated in. In most cases, the lower and upper range of macromolecules with different molecular weight overlaps, for example traces of catalase and ferritin are both found in fraction 3 (Figure 3.6B).

Using differential velocity ultracentrifugation through a 10 – 40% glycerol gradient, a range of molecular weight of the multimeric state of the recombinant T7-Vac14-HIS was obtained. Recombinant T7-Vac14-HIS was detected in fractions 1 – 4, with the strongest signal in fractions 2 and 3 (Figure 3.6A). Traces of recombinant T7-Vac14-HIS detected in fraction 1 that corresponds to phosphorylase b (~100 kDa) suggests a minimal presence of monomeric recombinant T7-Vac14-HIS. The majority of the recombinant T7-Vac14-HIS travelled beyond phosphorylase b suggesting that the recombinant T7-Vac14-HIS is self-interacting, forming a homomeric complex of greater than 100 kDa. The majority of the recombinant T7-Vac14-HIS were found in fractions 2 and 3, which corresponds to catalase, with a trail of signal into fraction 4 (Figure 3.6). The result is also consistent with previous data obtained by R.Botelho (Figure 4.1B). The S100 fraction containing vacuole membrane in yeast *fab1Δfig4Δ* double-mutant expressing Vac14-HA was subjected to differential velocity ultracentrifugation with 10 – 40%

glycerol gradient. The majority of Vac14-HA found in fraction 2 seems to be a dimer (Figure 4.1B). However, there is a long trail of signal into ferritin that is not seen with the recombinant T7-Vac14-HIS (Figure 3.6). The long trail observe of Vac14 from yeast lysates may represent interaction with other yeast proteins, even when FAB1 and FIG4 are deleted. For example, Vac14 also binds Vac7 and Atg18, which are also postulated to be involved in the regulation of PtdIns(3,5)P_2 [60]. In summary, results from glycerol gradient suggest that recombinant T7-Vac14-HIS can be either a homodimer (~200 kDa) and/or a homotrimer (~300 kDa).

4.5 Tandem purification of recombinant T7-Vac14-HIS

Analytical ultracentrifugation can be used to precisely identify the molecular weight and multimeric state of recombinant T7-Vac14-HIS. Analytical ultracentrifugation is based on the idea that when a strong centrifugal force is applied, macromolecules will migrate to the bottom of the solvent with a different rate of diffusion and sedimentation depending on the molecular weight of the monomeric and multimeric forms of the macromolecule. Analytical ultracentrifugation also combines computational software that monitors in real-time the rate of diffusion and sedimentation of the macromolecules. Combining the two, one can calculate the average molecular weight of the macromolecule and the association constant for macromolecule self-association. Therefore, monomeric macromolecules will have a different rate of diffusion and sedimentation compared to multimeric macromolecules. The analytical ultracentrifugation computes the average molecular weight and association constant based on a homogenous sample of macromolecules independent of the Stoke's radius. However, a homogeneous sample of recombinant T7-Vac14-HIS is required to proceed with analytical ultracentrifugation. The presence of degraded products from Ni^{2+}-NTA affinity chromatography will shift the average values generating false results (Figure 3.2B lane 2 (*) and Figure 3.7 lane 1 (*)).

To remove degradation products, recombinant T7-Vac14-HIS can be purified by binding the N-terminal T7 epitope to anti-T7 antibodies conjugated to agarose beads after purification through the HIS_6 purification. Therefore, anti-T7 conjugated to agarose beads was used to purify full-length recombinant T7-Vac14-HIS from the degraded products after Ni^{2+}-NTA purification (Figure 3.7 lane 1). Full-length recombinant T7-Vac14-HIS (~100 kDa) was indeed bound to anti-T7 conjugated to agarose beads and degraded products eliminated (Figure 3.7 lane 2). However, the affinity of the anti-T7 antibody for the T7-epitope of recombinant T7-Vac14-HIS is apparently very high, since full-length recombinant T7-Vac14-HIS was not eluted with multiple elutions with 1 mg/ml T7 peptide overnight (Figure 3.7 lane 3). Full-length recombinant T7-Vac14-HIS remained bound to anti-T7 antibody on the agarose beads (Figure 3.7 lane 4). Thus, another method was needed to effectively purify the full-length recombinant T7-Vac14-HIS from the degraded products and to recover recombinant Vac14.

4.6 Cloning and expression of recombinant T7-TEV-Vac14-HIS

To release the bound recombinant T7-Vac14-HIS, an oligonucleotide encoding a peptide sequence recognized by the TEV protease was cloned between the coding sequence for the T7 epitope and Vac14 (Figure 3.8). Recombinant T7-TEV-Vac14-HIS was successfully expressed and concentrated with Ni^{2+}-affinity chromatography (Figure 3.10). The TEV protease specifically recognizes and cleaves between the Gln-Gly sites of the peptide sequence Gl-Asn-Leu-Tyr-Phe-Gln-Gly. By cleaving this peptide region, recombinant Vac14-HIS should be released into the solvent, while the N-terminal T7 epitope should remain bound to the anti-T7 antibody conjugated to agarose. Purified recombinant Vac14-HIS will be used for analytical ultracentrifugation analysis (see Future Directions).

5. Future directions

This study suggests that recombinant T7-Vac14-HIS self-interacts to into a homodimer and/or homotrimer, which is consistent with previous research with mammalian and yeast. However, there are two outstanding issues to be resolved. First, analytical ultracentrifugation, will be used in the future to precisely define the multimeric state of Vac14 using homogenously pure recombinant Vac14. It was demonstrated in this study that the affinity of anti-T7 antibody for the N-terminal T7 epitope is very strong, thus, an alternate method to elute the full-length recombinant T7-Vac14-HIS was devised. Second, we need to elucidate the importance of multimeric Vac14 in the Fab1 complex. Is the Vac14 multimer necessary to form the Fab1 complex and regulate both the Fab1 kinase and Fig4 phosphatase?

The next step is to purify recombinant Vac14 for analytical ultracentrifugation analysis. Recombinant T7-TEV-Vac14-HIS was successfully expressed and concentrated by Ni^{2+}-affinity chromatography (Figure 3.10). Full-length recombinant T7-TEV-Vac14-HIS will be purified using anti-T7 antibody conjugated to agarose beads and subsequently cleaved by GST-TEV-HIS to elute recombinant Vac14-HIS. The GST-TEV-HIS will then be removed from solution by affinity chromatography with glutathione agarose beads (see purification of GST-fusion protein in methods and materials). Purified recombinant Vac14-HIS will be sent for analytical ultracentrifugation analysis at the Houry's Lab at the University of Toronto, Department of Biochemistry.

5.1 Analytical ultracentrifugation with sedimentation equilibrium

Analytical ultracentrifugation with sedimentation equilibrium (SE) will be used to validate the results obtained from velocity ultracentrifugation with glycerol gradients. SE is based on a similar concept to velocity ultracentrifugation with glycerol gradients, where a high

centrifugal force is applied to the molecule and the rate of migration of the molecule through the media depends on the molecular weight of the protein of interest [15, 52]. In addition, SE combines computational software to monitor the migration of molecules by refractive index changes and absorbance measurement from 200 to 800nm [52]. A wide concentration range of the molecules are examined simultaneously to identify the behaviour of the molecule in solution. Information regarding the oligomeric state and self-association constant can be then extrapolated [15, 37, 52].

5.2 Identifying the Vac14 self-interaction site

Ongoing research with the yeast system by my colleague, Tamadher Alghamdi, suggests that the C-terminal of Vac14 is responsible for self-interaction. Point mutants and truncations of recombinant Vac14 are currently being constructed. In-vitro interaction assay will be used to screen for recombinant Vac14 mutants that have lost the ability to interact with GST-Vac14. FPLC-SEC and differential velocity ultracentrifugation with glycerol gradients will be repeated with the recombinant Vac14 point mutants to observe if loss of interaction leads to a shift in fractionation. Once the precise location of the Vac14 self-interaction domain is identified, the information can be used for elucidating the importance of the multimeric Vac14 in the regulation of PtdIns(3,5)P_2.

5.3 Elucidating the importance of multimeric Vac14

To elucidate the importance of multimeric Vac14, a yeast strain deleted for *VAC14* can be transformed with the *vac14* point mutants that render Vac14 unable to self-interact. The *vac14Δ* yeast strain is deficient in PtdIns(3,5)P_2, which results in an enlarged vacuole [45]. We can then observe if *vac14* point mutants fused to GFP can localize to the vacuole or if they can rescue the localization of Fig4-GFP using fluorescence microscopy. Moreover, we can

investigate if the *vac14* point mutants that block multimerization can form the Fab1 complex, rescue PtdIns(3,5)P_2 synthesis and vacuolar morphology in *vac14Δ* yeast strain. At the conclusion of these studies, we should have a better appreciation of how Vac14 function in the regulation of PtdIns(3,5)P_2 and organelle function.

6. References

[1] Andrade, M.A., Petosa, C., O'Donoghue, S.I., Muller, C.W., Bork, P. (2001) Comparison of ARM and HEAT protein repeats J. Mol. Biol. 309, 1-18.

[2] Aniento, F. (1993) Cytoplasmic dynein-dependent vesicular transport from early to late endosomes [published erratum appears in J cell biol 1994 feb;124(3):397] J. Cell Biol. 123, 1373 - 1387.

[3] Anthony, L.C., Suzuki, H., Filutowicz, M. (2004) Tightly regulated vectors for the cloning and expression of toxic genes J. Microbiol. Methods. 58, 243-250.

[4] Backer, J.M. (2008) The regulation and function of class III PI3Ks: Novel roles for Vps34 Biochem. J. 410, 1-17.

[5] Bonangelino, C.J., Nau, J.J., Duex, J.E., Brinkman, M., Wurmser, A.E., Gary, J.D., Emr, S.D., Weisman, L.S. (2002) Osmotic stress-induced increase of phosphatidylinositol 3,5-bisphosphate requires Vac14p, an activator of the lipid kinase Fab1p J. Cell Biol. 156, 1015-1028.

[6] Botelho, R.J., Efe, J.A., Teis, D., Emr, S.D. (2008) Assembly of a Fab1 phosphoinositide kinase signaling complex requires the Fig4 phosphoinositide phosphatase Mol. Biol. Cell. 19, 4273-4286.

[7] BRAKKE, M. (1951) Density gradient centrifugation - a new separation technique. .

[8] Bright, N.A., Gratian, M.J., Luzio, J.P. (2005) Endocytic delivery to lysosomes mediated by concurrent fusion and kissing events in living cells Curr. Biol. 15, 360-365.

[9] Bryant, N.J., Piper, R.C., Weisman, L.S., Stevens, T.H. (1998) Retrograde traffic out of the yeast vacuole to the TGN occurs via the prevacuolar/endosomal compartment J. Cell Biol. 142, 651-663.

[10] Burnett, D., Wood, S.M., Bradwell, A.R. (1976) Estimation of the stokes radii of serum proteins for a study of protein movement from blood to amniotic fluid Biochim. Biophys. Acta. 427, 231-237.

[11] Canuel, M., Libin, Y., Morales, C.R. (2009) The interactomics of sortilin: An ancient lysosomal receptor evolving new functions Histol. Histopathol. 24, 481-492.

[12] Chow, C.Y., Landers, J.E., Bergren, S.K., Sapp, P.C., Grant, A.E., Jones, J.M., Everett, L., Lenk, G.M., McKenna-Yasek, D.M., Weisman, L.S., Figlewicz, D., Brown, R.H., Meisler, M.H. (2009) Deleterious variants of FIG4, a phosphoinositide phosphatase, in patients with ALS Am. J. Hum. Genet. 84, 85-88.

[13] Chow, C.Y., Zhang, Y., Dowling, J.J., Jin, N., Adamska, M., Shiga, K., Szigeti, K., Shy, M.E., Li, J., Zhang, X., Lupski, J.R., Weisman, L.S., Meisler, M.H. (2007) Mutation of FIG4 causes neurodegeneration in the pale tremor mouse and patients with CMT4J Nature. 448, 68-72.

[14] Christoforidis, S., McBride, H.M., Burgoyne, R.D., Zerial, M. (1999) The Rab5 effector EEA1 is a core component of endosome docking Nature. 397, 621-625.

[15] Cole, J.L., Lary, J.W., P Moody, T., Laue, T.M. (2008) Analytical ultracentrifugation: Sedimentation velocity and sedimentation equilibrium Methods Cell Biol. 84, 143-179.

[16] Cooke, F.T., Dove, S.K., McEwen, R.K., Painter, G., Holmes, A.B., Hall, M.N., Michell, R.H., Parker, P.J. (1998) The stress-activated phosphatidylinositol 3-phosphate 5-kinase Fab1p is essential for vacuole function in S. cerevisiae Curr. Biol. 8, 1219-1222.

[17] Cremona, O., Di Paolo, G., Wenk, M.R., Luthi, A., Kim, W.T., Takei, K., Daniell, L., Nemoto, Y., Shears, S.B., Flavell, R.A., McCormick, D.A., De Camilli, P. (1999) Essential role of phosphoinositide metabolism in synaptic vesicle recycling Cell. 99, 179-188.

[18] Di Paolo, G. and De Camilli, P. (2006) Phosphoinositides in cell regulation and membrane dynamics Nature. 443, 651-657.

[19] Doherty, G.J. and McMahon, H.T. (2009) Mechanisms of endocytosis Annu. Rev. Biochem. 78, 857-902.

[20] Donaldson, J.G. and Jackson, C.L. (2011) ARF family G proteins and their regulators: Roles in membrane transport, development and disease Nat. Rev. Mol. Cell Biol. 12, 362-375.

[21] Dong, X.P., Shen, D., Wang, X., Dawson, T., Li, X., Zhang, Q., Cheng, X., Zhang, Y., Weisman, L.S., Delling, M., Xu, H. (2010) PI(3,5)P(2) controls membrane trafficking by direct activation of mucolipin ca(2+) release channels in the endolysosome Nat. Commun. 1, 38.

[22] Dove, S.K., Cooke, F.T., Douglas, M.R., Sayers, L.G., Parker, P.J., Michell, R.H. (1997) Osmotic stress activates phosphatidylinositol-3,5-bisphosphate synthesis Nature. 390, 187-192.

[23] Dove, S.K., McEwen, R.K., Mayes, A., Hughes, D.C., Beggs, J.D., Michell, R.H. (2002) Vac14 controls PtdIns(3,5)P(2) synthesis and Fab1-dependent protein trafficking to the multivesicular body Curr. Biol. 12, 885-893.

[24] Dubin, P.L. and Principi, J.M. (1989) Failure of universal calibration for size-exclusion chromatography of rodlike macromolecules vs. random coils and globular proteins Macromolecules. 22, 1891 - 1896.

[25] Duex, J.E., Tang, F., Weisman, L.S. (2006) The Vac14p-Fig4p complex acts independently of Vac7p and couples PI3,5P2 synthesis and turnover J. Cell Biol. 172, 693-704.

[26] Efe, J.A., Botelho, R.J., Emr, S.D. (2005) The Fab1 phosphatidylinositol kinase pathway in the regulation of vacuole morphology Curr. Opin. Cell Biol. 17, 402-408.

[27] Efe, J.A., Botelho, R.J., Emr, S.D. (2007) Atg18 regulates organelle morphology and Fab1 kinase activity independent of its membrane recruitment by phosphatidylinositol 3,5-bisphosphate Mol. Biol. Cell. 18, 4232-4244.

[28] Ellson, C.D., Andrews, S., Stephens, L.R., Hawkins, P.T. (2002) The PX domain: A new phosphoinositide-binding module J. Cell. Sci. 115, 1099-1105.

[29] Ferguson, C.J., Lenk, G.M., Meisler, M.H. (2009) Defective autophagy in neurons and astrocytes from mice deficient in PI(3,5)P2 Hum. Mol. Genet. 18, 4868-4878.

[30] Gary, J.D., Sato, T.K., Stefan, C.J., Bonangelino, C.J., Weisman, L.S., Emr, S.D. (2002) Regulation of Fab1 phosphatidylinositol 3-phosphate 5-kinase pathway by Vac7 protein and Fig4, a polyphosphoinositide phosphatase family member Mol. Biol. Cell. 13, 1238-1251.

[31] Gary, J.D., Wurmser, A.E., Bonangelino, C.J., Weisman, L.S., Emr, S.D. (1998) Fab1p is essential for PtdIns(3)P 5-kinase activity and the maintenance of vacuolar size and membrane homeostasis J. Cell Biol. 143, 65-79.

[32] Godi, A., Di Campli, A., Konstantakopoulos, A., Di Tullio, G., Alessi, D.R., Kular, G.S., Daniele, T., Marra, P., Lucocq, J.M., De Matteis, M.A. (2004) FAPPs control golgi-to-cell-surface membrane traffic by binding to ARF and PtdIns(4)P Nat. Cell Biol. 6, 393-404.

[33] Gorelick, F.S. and Shugrue, C. (2001) Exiting the endoplasmic reticulum Mol. Cell. Endocrinol. 177, 13 -18.

[34] Groves, M.R. and Barford, D. (1999) Topological characteristics of helical repeat proteins Curr. Opin. Struct. Biol. 9, 383-389.

[35] Groves, M.R., Hanlon, N., Turowski, P., Hemmings, B.A., Barford, D. (1999) The structure of the protein phosphatase 2A PR65/A subunit reveals the conformation of its 15 tandemly repeated HEAT motifs Cell. 96, 99-110.

[36] Hales, C.M., Vaerman, J.P., Goldenring, J.R. (2002) Rab11 family interacting protein 2 associates with myosin vb and regulates plasma membrane recycling J. Biol. Chem. 277, 50415-50421.

[37] Hansen, J.C., Lebowitz, J., Demeler, B. (1994) Analytical ultracentrifugation of complex macromolecular systems. Biochemistry (American Chemical Society). 33, 13155-13163.

[38] Ho, C.Y., Alghamdi, T.A., Botelho, R.J. (2011) Phosphatidylinositol-3,5-bisphosphate: No longer the poor PIP(2) Traffic. .

[39] Hoepfner, S., Severin, F., Cabezas, A., Habermann, B., Runge, A., Gillooly, D., Stenmark, H., Zerial, M. (2005) Modulation of receptor recycling and degradation by the endosomal kinesin KIF16B Cell. 121, 437-450.

[40] Horiuchi, H., Giner, A., Hoflack, B., Zerial, M. (1995) A GDP/GTP exchange-stimulatory activity for the Rab5-RabGDI complex on clathrin-coated vesicles from bovine brain J. Biol. Chem. 270, 11257-11262.

[41] Hughes, W.E., Cooke, F.T., Parker, P.J. (2000) Sac phosphatase domain proteins Biochem. J. 350 Pt 2, 337-352.

[42] Ikonomov, O.C., Sbrissa, D., Fenner, H., Shisheva, A. (2009) PIKfyve-ArPIKfyve-Sac3 core complex: Contact sites and their consequence for Sac3 phosphatase activity and endocytic membrane homeostasis J. Biol. Chem. 284, 35794-35806.

[43] Ikonomov, O.C., Sbrissa, D., Foti, M., Carpentier, J.L., Shisheva, A. (2003) PIKfyve controls fluid phase endocytosis but not recycling/degradation of endocytosed receptors or sorting of procathepsin D by regulating multivesicular body morphogenesis Mol. Biol. Cell. 14, 4581-4591.

[44] Ikonomov, O.C., Sbrissa, D., Shisheva, A. (2001) Mammalian cell morphology and endocytic membrane homeostasis require enzymatically active phosphoinositide 5-kinase PIKfyve J. Biol. Chem. 276, 26141-26147.

[45] Jin, N., Chow, C.Y., Liu, L., Zolov, S.N., Bronson, R., Davisson, M., Petersen, J.L., Zhang, Y., Park, S., Duex, J.E., Goldowitz, D., Meisler, M.H., Weisman, L.S. (2008) VAC14 nucleates a protein complex essential for the acute interconversion of PI3P and PI(3,5)P(2) in yeast and mouse EMBO J. 27, 3221-3234.

[46] Kaiser, C. and Ferro-Novick, S. (1998) Transport from the endoplasmic reticulum to the golgi Curr. Opin. Cell Biol. 10, 477 - 482.

[47] Kippert, F. and Gerloff, D.L. (2009) Highly sensitive detection of individual HEAT and ARM repeats with HHpred and COACH PLoS One. 4, e7148.

[48] Koumandou, V.L., Dacks, J.B., Coulson, R.M., Field, M.C. (2007) Control systems for membrane fusion in the ancestral eukaryote; evolution of tethering complexes and SM proteins BMC Evol. Biol. 7, 29.

[49] Krauss, M., Kinuta, M., Wenk, M.R., De Camilli, P., Takei, K., Haucke, V. (2003) ARF6 stimulates clathrin/AP-2 recruitment to synaptic membranes by activating phosphatidylinositol phosphate kinase type igamma J. Cell Biol. 162, 113-124.

[50] Kumar, J., Yu, H., Sheetz, M. (1995) Kinectin, an essential anchor for kinesin-driven vesicle motility Science. 267, 1834- 1837.

[51] Lassing, I. and Lindberg, U. (1985) Specific interaction between phosphatidylinositol 4,5-bisphosphate and profilactin Nature. 314, 472-474.

[52] Lebowitz, J., Lewis, M., Schuck, P. (2002) Modern analytical ultracentrifugation in protein science: A tutorial review. .

[53] Lee, Y.H., Tan, H.T., Chung, M.C. (2010) Subcellular fractionation methods and strategies for proteomics Proteomics. 10, 3935-3956.

[54] Liu, Y., Boukhelifa, M., Tribble, E., Morin-Kensicki, E., Uetrecht, A., Bear, J.E., Bankaitis, V.A. (2008) The Sac1 phosphoinositide phosphatase regulates golgi membrane morphology and mitotic spindle organization in mammals Mol. Biol. Cell. 19, 3080-3096.

[55] Maire, M., Ghazi, A., Moeller, J., Aggerbeck, L. (1987) The use of gel chromatography for the determination of sizes and relative molecular masses of proteins. interpretation of calibration curves in terms of gel-pore-size distribution. Biochem. J. 243, 399-404.

[56] Majerus, P.W. and York, J.D. (2009) Phosphoinositide phosphatases and disease J. Lipid Res. 50 Suppl, S249-54.

[57] McCaffrey, M.W., Bielli, A., Cantalupo, G., Mora, S., Roberti, V., Santillo, M., Drummond, F., Bucci, C. (2001) Rab4 affects both recycling and degradative endosomal trafficking FEBS Lett. 495, 21-30.

[58] McLauchlan, H., Newell, J., Morrice, N., Osborne, A., West, M., Smythe, E. (1998) A novel role for Rab5-GDI in ligand sequestration into clathrin-coated pits Curr. Biol. 8, 34-45.

[59] McPherson, P.S., Garcia, E.P., Slepnev, V.I., David, C., Zhang, X., Grabs, D., Sossin, W.S., Bauerfeind, R., Nemoto, Y., De Camilli, P. (1996) A presynaptic inositol-5-phosphatase Nature. 379, 353-357.

[60] Michell, R.H. and Dove, S.K. (2009) A protein complex that regulates PtdIns(3,5)P2 levels EMBO J. 28, 86-87.

[61] Michell, R.H., Heath, V.L., Lemmon, M.A., Dove, S.K. (2006) Phosphatidylinositol 3,5-bisphosphate: Metabolism and cellular functions Trends Biochem. Sci. 31, 52-63.

[62] Morgan, J.R., Prasad, K., Hao, W., Augustine, G.J., Lafer, E.M. (2000) A conserved clathrin assembly motif essential for synaptic vesicle endocytosis J. Neurosci. 20, 8667-8676.

[63] Odorizzi, G., Babst, M., Emr, S.D. (1998) Fab1p PtdIns(3)P 5-kinase function essential for protein sorting in the multivesicular body Cell. 95, 847-858.

[64] Owen, D.J. (1998) A structural explanation for the recognition of tyrosine-based endocytotic signals Science. 282, 1327 - 1332.

[65] Raiborg, C., Bache, K.G., Gillooly, D.J., Madshus, I.H., Stang, E., Stenmark, H. (2002) Hrs sorts ubiquitinated proteins into clathrin-coated microdomains of early endosomes Nat. Cell Biol. 4, 394-398.

[66] Raiborg, C., Malerod, L., Pedersen, N.M., Stenmark, H. (2008) Differential functions of hrs and ESCRT proteins in endocytic membrane trafficking Exp. Cell Res. 314, 801-813.

[67] Robinson, F.L. and Dixon, J.E. (2006) Myotubularin phosphatases: Policing 3-phosphoinositides Trends Cell Biol. 16, 403-412.

[68] Rudge, S.A., Anderson, D.M., Emr, S.D. (2004) Vacuole size control: Regulation of PtdIns(3,5)P2 levels by the vacuole-associated Vac14-Fig4 complex, a PtdIns(3,5)P2-specific phosphatase Mol. Biol. Cell. 15, 24-36.

[69] Rusten, T.E., Vaccari, T., Lindmo, K., Rodahl, L.M., Nezis, I.P., Sem-Jacobsen, C., Wendler, F., Vincent, J.P., Brech, A., Bilder, D., Stenmark, H. (2007) ESCRTs and Fab1 regulate distinct steps of autophagy Curr. Biol. 17, 1817-1825.

[70] Rutherford, A.C., Traer, C., Wassmer, T., Pattni, K., Bujny, M.V., Carlton, J.G., Stenmark, H., Cullen, P.J. (2006) The mammalian phosphatidylinositol 3-phosphate 5-kinase (PIKfyve) regulates endosome-to-TGN retrograde transport J. Cell. Sci. 119, 3944-3957.

[71] Sbrissa, D., Ikonomov, O.C., Fenner, H., Shisheva, A. (2008) ArPIKfyve homomeric and heteromeric interactions scaffold PIKfyve and Sac3 in a complex to promote PIKfyve activity and functionality J. Mol. Biol. 384, 766-779.

[72] Sbrissa, D., Ikonomov, O.C., Fu, Z., Ijuin, T., Gruenberg, J., Takenawa, T., Shisheva, A. (2007) Core protein machinery for mammalian phosphatidylinositol 3,5-bisphosphate synthesis and turnover that regulates the progression of endosomal transport. novel sac phosphatase joins the ArPIKfyve-PIKfyve complex J. Biol. Chem. 282, 23878-23891.

[73] Sbrissa, D., Ikonomov, O.C., Strakova, J., Dondapati, R., Mlak, K., Deeb, R., Silver, R., Shisheva, A. (2004) A mammalian ortholog of saccharomyces cerevisiae Vac14 that associates with and up-regulates PIKfyve phosphoinositide 5-kinase activity Mol. Cell. Biol. 24, 10437-10447.

[74] Seabra, M.C., Mules, E.H., Hume, A.N. (2002) Rab GTPases, intracellular traffic and disease Trends Mol. Med. 8, 23-30.

[75] Stenmark, H., Aasland, R., Driscoll, P.C. (2002) The phosphatidylinositol 3-phosphate-binding FYVE finger FEBS Lett. 513, 77-84.

[76] Studier, F.W. and Moffatt, B.A. (1986) Use of bacteriophage T7 RNA polymerase to direct selective high-level expression of cloned genes J. Mol. Biol. 189, 113-130.

[77] Stulík, K. (2003) Some potentialities and drawbacks of contemporary size-exclusion chromatography J. Biochem. Biophys. Methods. 56, 1 - 13.

[78] Sweitzer, S.M. and Hinshaw, J.E. (1998) Dynamin undergoes a GTP-dependent conformational change causing vesiculation Cell. 93, 1021 - 1029.

[79] Takei, K., Mundigl, O., Daniell, L., De Camilli, P. (1996) The synaptic vesicle cycle: A single vesicle budding step involving clathrin and dynamin J. Cell Biol. 133, 1237-1250.

[80] Vetter, I.R., Arndt, A., Kutay, U., Gorlich, D., Wittinghofer, A. (1999) Structural view of the ran-importin beta interaction at 2.3 A resolution Cell. 97, 635-646.

[81] Vida, T.A. and Emr, S.D. (1995) A new vital stain for visualizing vacuolar membrane dynamics and endocytosis in yeast J. Cell Biol. 128, 779-792.

[82] Weissman, J.S., Kashi, Y., Fenton, W.A., Horwich, A.L. (1994) GroEL-mediated protein folding proceeds by multiple rounds of binding and release of nonnative forms Cell. 78, 693-702.

[83] Whyte, J.R. and Munro, S. (2002) Vesicle tethering complexes in membrane traffic J. Cell. Sci. 115, 2627-2637.

[84] Yamamoto, A., DeWald, D.B., Boronenkov, I.V., Anderson, R.A., Emr, S.D., Koshland, D. (1995) Novel PI(4)P 5-kinase homologue, Fab1p, essential for normal vacuole function and morphology in yeast Mol. Biol. Cell. 6, 525-539.

[85] Zhang, X., Chow, C.Y., Sahenk, Z., Shy, M.E., Meisler, M.H., Li, J. (2008) Mutation of FIG4 causes a rapidly progressive, asymmetric neuronal degeneration Brain. 131, 1990-2001.

[86] Zhang, Y., Zolov, S.N., Chow, C.Y., Slutsky, S.G., Richardson, S.C., Piper, R.C., Yang, B., Nau, J.J., Westrick, R.J., Morrison, S.J., Meisler, M.H., Weisman, L.S. (2007) Loss of Vac14, a regulator of the signaling lipid phosphatidylinositol 3,5-bisphosphate, results in neurodegeneration in mice Proc. Natl. Acad. Sci. U. S. A. 104, 17518-17523.

[87] Zoncu, R., Perera, R.M., Balkin, D.M., Pirruccello, M., Toomre, D., De Camilli, P. (2009) A phosphoinositide switch controls the maturation and signaling properties of APPL endosomes Cell. 136, 1110-1121.